

# Chemical composition of post-AGB star candidates

R. E. Molina<sup>1,\*</sup> C. B. Pereira<sup>2</sup> and A. Arellano Ferro<sup>3</sup>

<sup>1</sup> Laboratorio de Investigación en Física Aplicada y Computacional, Universidad Nacional Experimental del Táchira, Venezuela.

<sup>2</sup> Observatório Nacional/MCTI, Rua Gen. José Cristino 77, Sao Cristovao, Rio de Janeiro, CEP 20921-400, Brazil.

<sup>3</sup> Instituto de Astronomía, Universidad Nacional Autónoma de México, Ciudad de México, CP 04510, México.

Received XXXX, accepted Jan 16, 2019

Published online XXXX

**Key words** stars: abundances - stars: post-AGB stars.

We present a high resolution detailed abundance analysis for a sample of six post-AGB candidate stars, five of them had not been studied spectroscopically in the optical region. All the analyzed objects are IRAS sources identified as possible post-AGB on the two-colours IRAS diagram. We find three objects with clear signs of evolved stars; IRAS 05338-3051 shows abundances similar to the RV Tauri V453 Oph; the lower-luminosity stars IRAS 18025 - 3906 is O-rich without s-process enrichment and IRAS 18386 - 1253 shows a moderate selective depletion of refractory elements generally seen in post-AGB stars, which show mid-IR excess; they may be evolved post-RGB objects, in which case these would be the first Galactic counterparts of post-RGB objects observed in the Large and Small Magellanic Clouds (Kamath et al. 2014, 2015). On the other hand, IRAS 02528 + 4350 seems to be a moderately metal-poor young object and IRAS 20259 + 4206 also seems to be a young object showing carbon deficiency; however, an analysis with better spectra might be in order to clarify its evolutionary state. Finally, our abundances calculations for the binary post-AGB star IRAS 17279 - 1119 are found in good agreement with those of De Smedt et al. (2016).

Copyright line will be provided by the publisher

## 1 Introduction

Post-AGB stars (PAGBs) are luminous objects of low-to intermediate-mass (0.8–8.0  $M_{\odot}$ ) in the late stages of their evolution. These objects are located in the intermediate evolutionary stages between the end of the AGB phase and the beginning of the planetary nebulae (PN). They display diverse chemical atmospheric compositions as they are determined by nucleosynthesis and mixing processes and by extensive mass loss occurring during the AGB phase of evolution (Iben & Renzini, 1983; Karakas et al., 2014; Marigo et al., 2013). The structure and evolution of low and intermediate mass stars during the AGB and the PAGB phases has been described in detail in numerous papers (e.g. Bloeker, 1995; Busso et al., 1999; Herwig, 2005; Vassiliadis & Wood, 1993). It is clear now that severe mass loss at the end of AGB leads to enrichment of the interstellar medium in carbon, nitrogen and s-process elements (e.g. Dray et al., 2003; Iben & Truran, 1978; Karakas, 2010). Hence, AGB stars play a very important role in the chemical evolution of the galactic interstellar medium.

In massive AGB stars, heavy mass loss produces a dense circumstellar shell that obscures the central regions whereas the central star may remain at least partially visible. The dust in the circumstellar shells is heated by stellar radiation, and causes an infrared (IR) excess. Hence, the optically visible galactic PAGBs generally exhibit two

peaks in their spectral energy distribution (SED) and could be separated accordingly into two groups of SEDs: disk-sources (de Ruyter et al., 2006; Gielen et al., 2009; van Winckel et al., 2009) and shell-sources (van Winckel, 2003). The first group displays SEDs with a broad IR excess starting in the near-IR region, which point to the presence of hot dust near the central star (these objects are associated with binary stars). The second group contains PAGBs with a double-peaked SED where the first peak corresponds to the photospheric flux and the second peak represents the IR emission of an expanding dusty envelope (these objects are single stars).

Some subgroups of PAGBs with IR-excess may be identified according to their C/O ratio being either greater or smaller than one. A good account of the progress in our understanding of PAGBs can be found in the works of van Winckel (2003), García-Lario (2006) and Giridhar (2011). PAGBs in LMC and SMC have been studied and summarized by van Aarle et al. (2011), van Aarle et al. (2013) and Kamath et al. (2014). Their known distances allow good estimates of their luminosity and mass. From their chemical composition PAGBs can also be distinguished for example by the s-process enhancement (e.g. Reyniers et al., 2007) and by the depletion of condensable elements (e.g. Gielen et al., 2009). For a more recent summary of galactic and extra-galactic PAGBs see De Smedt et al. (2016) and the references therein. In these studies some inadequacies of theoretical AGB models in explaining the observed low C/O

\* Corresponding author: rmolina@unet.edu.ve

ratios in s-process enriched stars (De Smedt et al., 2014, 2012; van Aarle et al., 2013) and the low upper limit of Pb are remarked (De Smedt et al., 2014).

PAGBs with  $C/O > 1$ , e.g. HD 56126, HD 187785 and IRAS 06530-0213 display a considerable enhancement of C and s-process elements (e.g. Reddy et al., 2002; Reyniers et al., 2002, 2004; Van Winckel et al., 1997). PAGBs exhibiting s-process elements caused by the third dredge-up (TDUP) make only a small fraction of the known PAGBs and they are generally single stars.

PAGBs with  $C/O < 1$ , e.g. 89 Her, HD 161796, HD 133656, SAO 239853, etc, are O-rich and do not display s-process enhancement, whilst many PAGBs with  $C/O \sim 1$  e.g. BD + 39 4926, HR 4049, HD 44179, HD 46703, HD 52961 (van Winckel, 2003; Van Winckel et al., 1995) show abundance peculiarities caused by selective removal of condensable elements. This selective removal of refractory elements has been attributed to the presence of a stellar companion and the circumstellar envelope that provides the site for dust-gas separation to take place. Re-accretion of clean gas from the circumbinary shell to the photosphere, while the dust remains stable in the circumstellar shell (due to large radiation pressure on them), results in anomalous chemical composition exhibited by these objects. This scenario, proposed by Venn & Lambert (1990), Bond (1991) and elaborated by Waters et al. (1992), has been gaining support through the observed depletions of condensable elements in a large number of PAGBs, including RV Tauri stars (Giridhar et al., 2000, 2005, 1994; Gonzalez et al., 1997; Van Winckel et al., 1997, 1995). Studies of extended samples of PAGBs, including RV Tauri stars with dusty disk, have been carried out by Maas et al. (2002) and de Ruyter et al. (2006) and the chemical anomalies arising due to depletion of condensable elements is observed at various degrees, which further supports the above mentioned hypothesis. Binary companions are detected for a large number of PAGBs showing depletions and a sizable fraction of them being RV Tauri stars. The presence of a dusty disk, generally inferred from the shape of their SED, is also supported by mid-IR interferometry (Deroo et al., 2006), which points towards the existence of compact disks. Through time series radial velocity monitoring, van Winckel et al. (2009) computed the orbital elements of many PAGB binaries showing removal refractory elements depletions.

A detailed study of a set of RV Tauri and PAGBs based on the analysis of their SED (shell and disk sources) carried out by Gezer et al. (2015), has shown that there is a correspondence between the properties of the SED and binarity. These authors noted a complex relationship between the IR properties and chemical anomaly and they reported that all confirmed binaries are disk sources but not all of them show depletion patterns.

However, among depleted sources there are some objects with apparently no IR excess. An example is the heavily depleted object BD + 39 4926. The depletion effect could be explained by its binary nature in spite of a lack of de-

tected IR excess. According to Gezer et al. (2015) the depleted photosphere remains chemically peculiar for a longer time than the IR excess remains detectable.

However, Venn et al. (2014), using new photometry data taken from WISE database, have demonstrated that BD + 39 4926 has a mild-IR excess beyond 10 microns. The radial velocity curve of BD + 39 4926 together with orbital parameters was obtained by Gezer et al. (2015).

The IRAS two colour diagram and the  $J - K$  versus  $H - K$  diagram have been very useful tools in identifying new source candidates to PAGBs and PN (García-Lario et al., 1997; Preite-Martinez, 1988; van der Veen & Habing, 1988). However, the confirmation of these sources as PAGBs, requires detailed chemical composition analysis from high-resolution spectroscopy. The extensive IRAS source list studied by García-Lario et al. (1997) and its refinement in the optical from low-resolution spectroscopy by Suárez et al. (2006) and Pereira & Miranda (2007), have contributed to the identification of new candidate objects to PAGBs. More recently, Szczerba et al. (2017) show the results of the search of new AGB (2,510) and PAGB (24,821) star candidates using the [3.4]-[12] vs [4.6]-[22] two colour diagram from ALLWISE photometry.

Although the number of known PAGBs has grown considerably, their chemical diversity, particularly among objects of very similar atmospheric parameters, highlights the complexities involved and our limited understanding of the processes operating during the relatively fast AGB and PAGB evolution. Hence, identification, detailed atmospheric analysis and SED properties of new PAGB stars is important in providing observational constraints to refine the models of PAGB evolution, including the influence of binary companions.

In continuation of our search and analysis of new candidates to PAGBs (Giridhar et al., 2010; Molina et al., 2014), in the present paper we carry out a high resolution detailed abundance analysis for a sample of five candidate objects; IRAS 02528 + 4350, IRAS 05338 - 3051, IRAS 18025 - 3906, IRAS 18386 - 1253 and IRAS 20259 + 4206, selected via the IRAS two colour diagram, and of the binary post-AGB star IRAS 17279-1119.

This work is structured as follows; in Section 2 we describe the selection process of our sample. In Section 3 we give a description of the observations. In Section 4 the initial atmospheric parameters calculation is described. In Section 5, the methodology towards the abundances calculation and their uncertainties is presented. In Section 6, we report the individual abundances for each star in our sample. Section 7 is dedicated to the discussion of the implications of the chemical results on the status of each objects, and finally we summarize our conclusions in Section 8.

## 2 THE SAMPLE

The IRAS two colour diagram (García-Lario et al., 1997; van der Veen & Habing, 1988) has been very

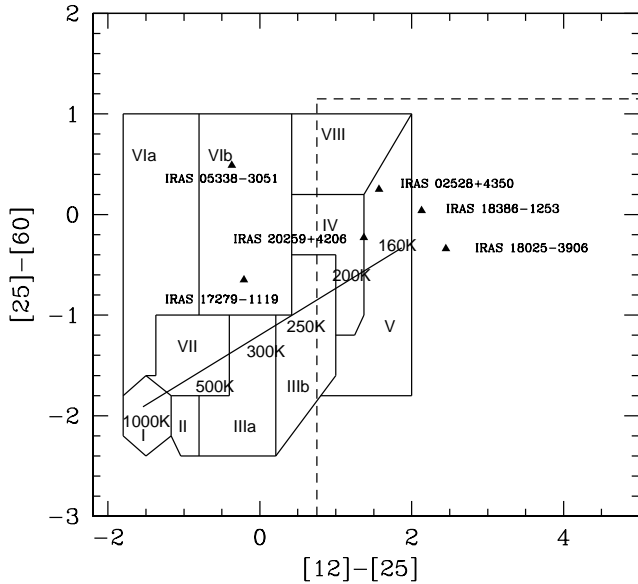


**Fig. 1** Location of the sample stars in the IRAS two colour diagram. The dotted-line represents the PNs and PAGBs region limited by García-Lario et al. (1997). The different regions represented with roman numerals have been defined by van der Veen & Habing (1988) and separate stars by the dust/gas ratio in the envelope. The black body curve is represented by the straight line.

useful in separating and identifying different types of luminous evolved stars, in particular those in the post-AGB evolutionary phases (see Fig. 1). The present sample contains the stars IRAS 02528 + 4350, IRAS 05338 - 3051, IRAS 17279 - 1119, IRAS 18025 - 3906, IRAS 18386 - 1253 and IRAS 20259 + 4206. Four of them IRAS 02528 + 4350, IRAS 18025 - 3906, IRAS 18386 - 1253 and IRAS 20259 + 4206 fall within the region for PNs and PAGBs defined by García-Lario et al. (1997), and the other two IRAS 05338 - 3051 and IRAS 17279 - 1119, fall in the VIb region which, according to van der Veen & Habing (1988) contains variable stars with relatively hot dust closer to the star and colder dust at larger distances. A brief review of the six objects is given below.

IRAS 02528 + 4350 (GLMP 34) is a high-latitude galactic object and was included in the sample of Preite-Martínez (1988) as a PN candidate. Preite-Martínez derived a dust temperature of 132K and estimated a distance of 3.8 kpc. This object was included as an IRAS galaxy due to its IR-excess at 60 $\mu$ m band (Cohen, 1992; Nakanishi et al., 1997). With  $[12] - [25] = +1.57$  and  $[25] - [60] = +0.25$ , it belongs to the zone of PAGBs defined by García-Lario et al. (1997). Suárez et al. (2006), using low-resolution spectra, classified it as a young object of the A0e spectral type. Szczerba et al. (2007) included it in Toruń catalogue as possible a PAGB object. Vickers et al. (2015) proposed that it belongs to population of the thin disk, and adopting a core mass of  $0.53 \pm 0.02 M_{\odot}$ , through the core mass–luminosity

relation of Vassiliadis & Wood (1993), found a luminosity of  $L_* \approx 1700 \pm 750 L_{\odot}$  and a distance of  $4.34 \pm 0.98$  kpc.

IRAS 05338 - 3051 (RV Col) is of high galactic latitude ( $b = +28.8$ ), with spectral type G5 I (Straizys, 1982) and without an IR-excess observed. It is classified as a semi-regular variable in the General Catalog of Variable Stars (GCVS). Hoffmeister (1943) reports a period of 105.7 days. Light curves for different photometric bands indicate that the period is relatively stable with an amplitude of  $\sim 0.8$  mag in the V-band, but according to Eggen (1986) it displays a "malformation" near 25 days after maximum light.

The star has been monitored for about 9 years by the All-Sky Automated Survey (ASAS-3) group. The light curve includes 600 observations which exhibit a stable sinusoidal light variation with a variable amplitude of 0.5 to 1.0 mag. Arkhipova et al. (2011) found two active periods in the light variations;  $105.8 \pm 1.0$  and  $108.6 \pm 1.5$  days with a maximum amplitude of 0.6 mag. Although the amplitude varies, the period has remained almost constant for decades (Arkhipova et al., 2011).

Trams et al. (1991) pointed out that this object does not show infrared excesses and suggested it to be a red giant of spectral type G. van der Veen et al. (1993) studied the mass-loss rate and the expansion velocity for a set of evolved stars, including IRAS 05338 - 3051, however, the rotational molecular lines of  $^{12}\text{CO}$  J = 1-0 and J = 2-1 were not sufficiently intense for a detailed analysis of this object.

IRAS 05338 - 3051 is listed as a possible PAGBs into the Toruń catalogue of post-AGB stars (Szczerba et al., 2007). Vickers et al. (2015) estimated a distance of  $2.42 \pm 0.52$  kpc from an adopted luminosity of  $3500 \pm 1500 L_{\odot}$ . According to Vickers et al. this object probably belongs to the old thin disk population. The IRAS colours  $[12] - [25] = -0.37$  and  $[25] - [60] = +0.51$  show that this object falls in the VIb region of the colour-colour diagram of van der Veen & Habing (1988).

IRAS 17279 - 1119 (HD 158616) has been the subject of several abundance analysis e.g. Van Winckel (1997), Arellano Ferro et al. (2001), S. S. Rao et al. (2012), De Smedt et al. (2016). Bogaert (1994) identified two possible periods between 61 and 93 days for this star. Van Winckel (1997) points out that the optical photometry shows similarity to RV Tauri stars. With  $[12] - [25] = -0.21$  and  $[25] - [60] = -0.65$ , it belongs to the zone VIb. This object has also been included in the Toruń Catalogue of Galactic PAGB (Szczerba et al., 2007) as a likely PAGBs.

An extensive monitoring of the radial velocity for about  $\sim 6$  yr (Gorlova et al., 2015; Van Winckel et al., 2010) led to determination of the radial velocity orbit. De Smedt et al. (2016) also used the ASAS-3 photometry and found periods between 83 and 90 days. The SED constructed from different photometric sources by De Smedt et al. (2016) (their figure 16) shows an infrared excess starting near 2 microns, which is indicative of the presence of warm dust at sublimation temperature near the central star. It has been suggested by several workers (Bujarrabal et al., 2015; de Ruyter et al.,

2006; Deroo et al., 2007; Gezer et al., 2015; Gielen et al., 2011; Hillen et al., 2014, 2013) that this is caused by a stable compact circumbinary disk.

IRAS 18025 - 3906 (GLPM 713) was included in the sample of Prite-Martinez (1988) as a PN candidate. However, from their analysis they concluded that IRAS 18025 - 3906 is not a PN but that the object appears to be a non-variable OH/IR star and a proto-planetary nebulae (PPN) candidate. The author derived a dust temperature of 172 K for this object. Hu et al. (1993) relate IRAS 18025 - 3906 to the optical counterpart object with a G2 I spectral type. In addition these authors detected OH-masers at 1612 and 1667 MHz and its SED shows a double-peak structure (see their Fig. 3, item # 40).

Silva et al. (1993) detected a double peaked OH-maser emission at 1612 MHz with velocities of  $-103$  and  $-130$  km  $s^{-1}$ . They estimated a velocity (LSR) of  $-116$  km  $s^{-1}$ , an envelope expansion velocity of  $13$  km  $s^{-1}$ , a mass loss rate of  $M = 5.0 \times 10^{-6} M_{\odot} \text{ yr}^{-1}$  and a luminosity of  $L_{*} = 201 L_{\odot}$  and concluded that the star is probably a PPN. The IRAS colours  $[12] - [25] = +2.45$  and  $[25] - [60] = -0.34$  indicate that the star falls into the region defined by García-Lario et al. (1997). The PAGB nature of IRAS 18025 - 3906 with its optical counterpart has been confirmed by Suárez et al. (2006) using low-resolution spectra and is classified as a G1 I star. Vickers et al. (2015) found a distance of  $5.20 \pm 0.70$  kpc from an adopted luminosity of  $6000 \pm 1500 L_{\odot}$  respectively, locating this object probably at intermediate thin disk population. The star has been monitored by the ASAS-3, the light curve includes 490 observations and does not show signs of a periodic variation.

IRAS 18386 - 1253 (GLPM 818) is a relatively unexplored object. Its IRAS colours  $[12] - [25] = +2.13$  and  $[25] - [60] = +0.04$  place the object into the PAGBs-PNs region in Fig. 1. This object has also been included in the Toruń Catalogue of Galactic PAGB (Szczerba et al., 2007) as a likely PAGBs. Pereira & Miranda (2007) classified the star as a PAGB by comparing its spectrum with that of the known PAGB GLMP 1078 and they assigned its spectral type as F5 I. Vickers et al. (2015) found a distance of  $6.83 \pm 1.03$  kpc from an adopted luminosity of  $6000 \pm 1500 L_{\odot}$ . Likewise IRAS 18025 - 3906, IRAS 18386 - 1253 is classified as a possible intermediate thin disk population object. It has also been monitored for a long time by ASAS-3; its light curve includes some 539 observations. It does not display a periodic variation although it may have a characteristic time of variation of about a hundred days.

IRAS 20259 + 4206 (GLPM 998) was studied by Suárez et al. (2006) using low-resolution spectra and classified it as a F3 I PAGB star. It was also recorded as a likely PAGB in the Toruń Catalogue (Szczerba et al., 2007). A failed search of  $H_2O$  and  $SiO$  masers in its envelope is reported by Suárez et al. (2007) and Yoon et al. (2014). Vickers et al. (2015) considers this object as of the intermediate thin disk population.

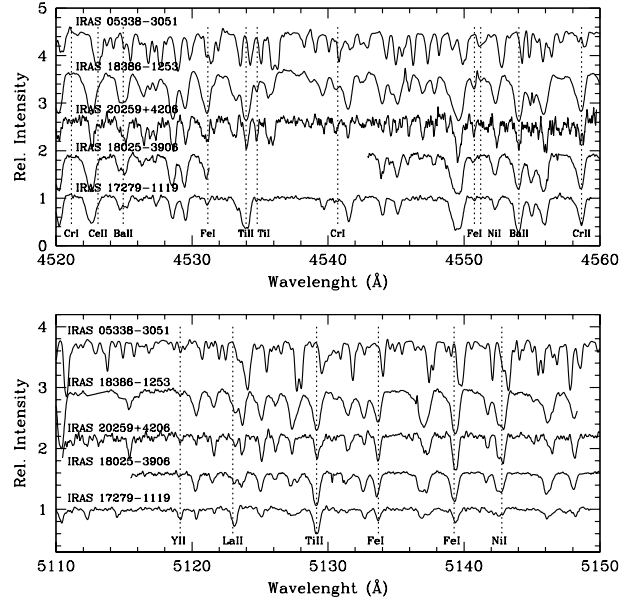


**Fig. 2** Representative spectra of the sample stars IRAS 05338 - 3051, IRAS 17279 - 1119, IRAS 18025 - 3906, IRAS 18386 - 1253 and IRAS 20259 + 4206 of two different regions. The location of lines of certain important elements have been indicated by dashed lines. The stars are arranged in increasing order the effective temperature (top to bottom).

It is clear that a detailed abundance analysis based on high resolution spectra for all these objects is key in order to confirm their evolutionary status.

In Table 1 we list the equatorial and galactic coordinates, the  $V$  magnitude, and IRAS fluxes for the stars in our sample.

### 3 Observations

The spectra used in the present work were obtained at different observatories with a variety of high resolution spectrographs: The Fiber-fed Extended Range Optical Spectrograph (FEROS) mounted at the 2.2m telescope at La Silla Observatory (Chile); the Fibre-fed Echelle Spectrograph (FIES) mounted on the 2.5m Nordic Optical Telescope (NOT) at the Roque de los Muchachos Observatory at La Palma (Spain), the Tull echelle spectrograph (Tull et al., 1995) on the 2.7m telescope at the McDonald Observatory (USA), and the Hanle Echelle Spectrometer (HESP) mounted on the 2m optical-infrared Himalayan Chandra Telescope (HCT) at the Indian Astronomical Observatory (IAO) (India).

IRAS 02528 + 4350 and IRAS 17279 - 1119 were observed on the nights of April 26, and October 20, 2016. Two exposures were obtained for each object to improve the S/N ratio. These spectra obtained with HESP cover the  $3660\text{-}10550\text{Å}$  range and have a resolution power of  $R(\lambda/\Delta\lambda) \sim 60,000$ .

**Table 1** Basic data of the program stars. Numbers in parenthesis are the uncertainties in the flux.

No. IRAS	$\alpha_{2000}$ (h m s)	$\delta_{2000}$ (h m s)	$V$ (mag)	$l$ ( $^{\circ}$ )	$b$ ( $^{\circ}$ )	$F_{12 \mu\text{m}}$ (Jy)	$F_{25 \mu\text{m}}$ (Jy)	$F_{60 \mu\text{m}}$ (Jy)	$F_{100 \mu\text{m}}$ (Jy)
02528 + 4350	02 56 11.3	+44 02 52.1	10.68	145.41	-13.30	0.56(3)	2.38(3)	3.00(2)	2.22(1)
05338 - 3051	05 35 44.2	-30 49 35.3	9.30	234.98	-28.78	0.35(3)	0.25(1)	0.40(1)	1.00(1)
17279 - 1119	17 30 46.9	-11 22 08.3	9.68	013.23	-12.17	3.52(3)	2.90(3)	1.60(3)	1.98(1)
18025 - 3906	18 06 03.2	-39 05 56.6	11.73	353.26	-8.72	4.30(3)	41.20(3)	30.11(3)	7.68(3)
18386 - 1253	18 41 28.8	-12 50 52.0	13.10	20.36	-3.65	1.43(3)	10.19(3)	10.62(3)	48.27(1)
20259 + 4206	20 27 41.9	+42 16 42.0	13.75	80.39	+2.19	2.49(3)	8.82(3)	7.01(3)	135.40(1)

IRAS 05338 - 3051 was observed on February 10, 2017 with the Tull spectrograph of McDonald Observatory. Three exposures were combined to increase the S/N ratio. They cover a range of wavelength of 3650–10350 Å and a resolution of ~60,000.

IRAS 18025 - 3906 and IRAS 18386 - 1253 were observed on September 30, 1998 and July 29, 2009 respectively. Their spectra were obtained with the Fiber-fed Extended Range Optical Spectrograph (FEROS) and cover a range of wavelength of 3900–9200 Å with a resolution of  $R \sim 48,000$ . These spectra form part of the same collection of objects studied by Molina et al. (2014).

IRAS 20259 + 4206 was observed on June 24, 2014. Five spectra were obtained with an exposure time of 1800 secs each. Individual spectra have a S/N ~15. The combined spectrum has a S/N ~30. The wavelength range obtained with FIES is 3650–7150 Å and it is distributed in 78 orders with a resolution  $R \sim 25,000$ . The spectra were reduced following the standard procedure and summed using the task COMBINE= MEDIAN to remove the cosmic ray hits. Because of the low signal-to-noise only a limited number of line strengths for each identified elements were measured.

As a comparison, two 40 Å regions, are displayed in Fig. 2 for each of the spectra of the sample stars. The vertical dotted lines represent the positions at rest of some absorption lines of elements such as Y II, La II, Ti II, Fe I, Ba II, Cr II, Cr I and Ni I present in these spectral regions. In the two spectral regions shown in Fig. 2, the star IRAS 05338 - 3051 is not present because its spectral features are very weak and barely detectable.

#### 4 ATMOSPHERIC PARAMETERS

The shape and strength of spectral lines depend strongly on the physical conditions prevailing in the atmosphere of the star. Hence, good estimates of effective temperature,  $T_{\text{eff}}$ , surface gravity,  $\log g$ , and microturbulence velocity,  $\xi_t$  are necessary to derive accurate abundances. First estimates of these atmospheric parameters can be made from different approaches.

For the effective temperature a first approach can be obtained for example from the spectral type and the calibrations of Schmidt-Kaler (1982). Spectral types can be generally be found in the SIMBAD database and/or from the work of Suárez et al. (2006). Our calculations of  $T_{\text{eff}}$  are 9730K (~A0) for IRAS 02528 + 4350, 4850K (~G5) for IRAS 05338 - 3051, 7350K (~F2/3) for

IRAS 17279 - 1119, 5200K (~G2) for IRAS 18025 - 3906, 6900K (~F5) for IRAS 18386 - 1253 and 7200K (~F3) for IRAS 20259 + 4206.

A second approach to the effective temperature calculation is from the spectroscopy calibrations of Molina (2018) for PAGB stars. These calibrations enable to estimate the  $T_{\text{eff}}$ , from the equivalent widths of specific absorption lines. For stars of intermediate temperature, we employed the equivalent width of Ca IIK at 3933 Å, while for cooler stars the G-band at 4302 Å and Ca I at 4226 Å are used. From the sample studied,  $T_{\text{eff}}$  could be calculated by this approach for IRAS 02528 + 4350 and IRAS 18025 - 3906, obtaining the values  $7981 \pm 91\text{K}$  and  $6196 \pm 91\text{K}$  respectively. The remaining objects do not have the above features in the observed spectral range.

A third independent approach to estimate  $T_{\text{eff}}$ , and  $\log g$ , is from the Balmer lines profile fitting (Venn, 1995). Theoretical Balmer profiles have been synthesized using the SPECTRUM<sup>1</sup> code and a grid of ODFNEW model atmospheres (Castelli & Kurucz, 2003), and were used to fit the observed profiles of H $\beta$  and H $\delta$ . The solution is not unique as different pairs of  $T_{\text{eff}} - \log g$  may produce a good line fit. A locus of good solutions can be seen on the  $T_{\text{eff}} - \log g$  plane. As underlying core emission may be present in some stars, we chose to fit only the wings of the Balmer lines. Additional loci are obtained by searching for  $T_{\text{eff}} - \log g$  pairs that yield consistent abundance for neutral and ionized lines of Mg I/Mg II, Si I/Si II, Sc I/Sc II, Ti I/Ti II, and Cr I/Cr II.

The intersection of these loci gives good estimates of the temperature and gravity. For some stars however, the emission is so conspicuous that this criterion can not be used. We have shown in Fig. 3 the loci of temperatures and gravities derived using different species mentioned above. The adopted values for the temperature and gravity are indicated by the filled circle. With this method we estimated the initial value ranges of temperature and gravity for IRAS 18025 - 3906 (6125–6335 K, 0.1–0.4) and for IRAS 20259 + 4206 (5820–6380 K, 1.9–2.4). IRAS 02528 + 4350 a single solution (8441 K; 1.13) is obtained from the intersection of H $\beta$  and H $\delta$  loci. The differences between the values adopted (7900 K; 2.40) and the estimated from the intersection between the loci of the Balmer lines might be due to the poor quality of the observed spectrum. For the remaining objects, the Balmer profiles are polluted by emission and could also affect the estimates of both parameters. The values of temperature and gravity were obtained by the intersection

<sup>1</sup><http://www.appstate.edu/~grayro/spectrum/spectrum.html>

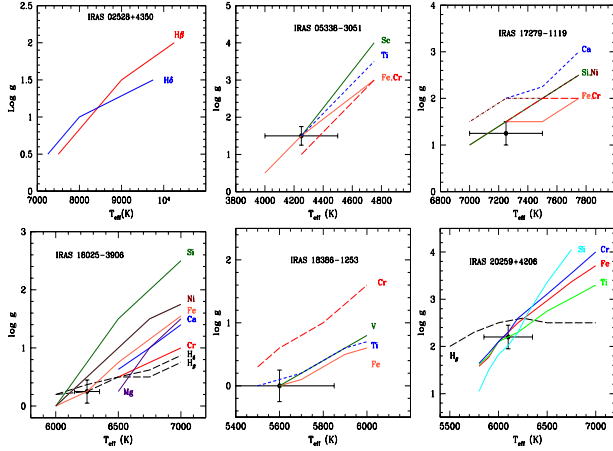


**Fig. 3** Locus of different solutions are represented on the  $T_{\text{eff}}-\log g$  plane for each star of the sample. The filled circle with error bars indicate the adopted initial values of  $T_{\text{eff}}$  and  $\log g$  for the subsequent calculation of abundances. The colour version of this figure can be seen online.

of loci of different species with two states of ionization. For IRAS 05338 - 3051 (4000–4500 K; 1.22–1.68) were estimated from the intersection between the Ti, Sc and Fe loci, for IRAS 17279 - 1119 (7000–7500 K; 1.0–1.4) from Si, Fe and Cr loci, and for IRAS 18386 - 1253 (5400–5850 K; 0.0–0.2) from Ti, V and Fe loci respectively. These initial estimates of  $T_{\text{eff}}$  and  $\log g$  shall be refined by a detailed spectral analysis.

For the detailed abundance analysis, we employed the 2015 version of the spectral code MOOG (Snedden, 1973) along with the grids of LTE plane-parallel ODFNEW model atmospheres.

Temperature and gravity can be estimated from accurate measurements of equivalent widths (EWs) for a set of Fe lines with well determined atomic data ( $\log gf$  and  $\chi$  (eV)). We restricted to EWs with values between 10 to 200 mÅ to avoid NLTE effects on strong lines. By eliminating the dependence of calculated abundances on lower excitation potentials and requiring that the neutral and ionized lines give the same abundances, i.e.  $\log n(\text{Fe I}) = \log n(\text{Fe II})$  one can get good estimates of  $T_{\text{eff}}$ ,  $\log g$  respectively. In order to confirm the value of gravity, the equilibrium condition can be extended to other elements with two ionization states (such as Mg, Si, Ca, Ti, Cr, Ni). The microturbulence velocity was estimated by requiring that the derived abundances are independent of line strengths. In addition we can confirm the microturbulence velocity value by plotting  $\sigma_X$  vs.  $\xi_t$  and following the method described in Şahin & Lambert (2009). Standard deviation for elements like Fe, Si and Cr leads to a minimum value of microturbulence velocity in the 0 to 8  $\text{kms}^{-1}$  range. Fig. 4 illustrates the method for the star IRAS 18025 - 3906, in which a minimum error for  $\xi_t$  of  $\sim 4.0$   $\text{kms}^{-1}$  is found.

An error in the EWs of about 8 to 10%, corresponds to an uncertainty in the effective temperature of  $\pm 250$  K, to

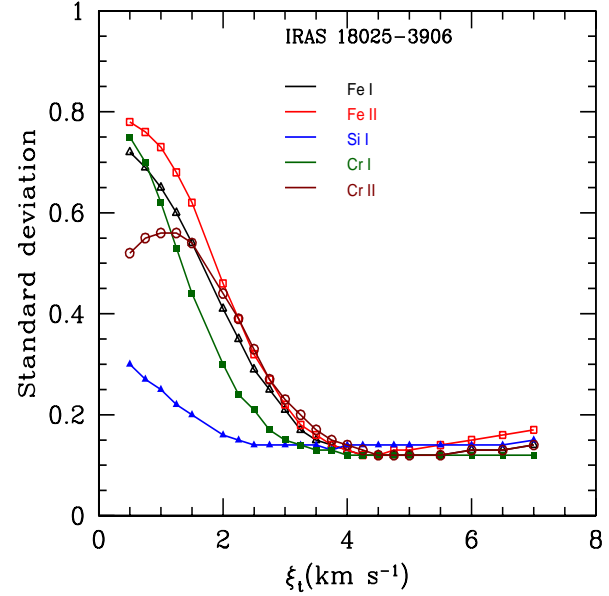


**Fig. 4** Determination of microturbulence velocity for the star IRAS 18025 - 3906 using the plot of standard deviation as a function of microturbulence velocity  $\xi_t$  for several species in the 0 to 8  $\text{kms}^{-1}$  range. The colour figure can be viewed in the online version.

$\pm 0.25$  in the superficial gravity and to  $\pm 0.5$   $\text{kms}^{-1}$  in the microturbulence velocity of  $\pm 0.5$   $\text{kms}^{-1}$ . Our final adopted values of the atmospheric parameters for the stars in our sample are listed in Table 2.

## 5 DETERMINATION OF ATMOSPHERIC ABUNDANCES

In the determination of atmospheric chemical abundances we use the equivalent widths of 141, 152, 205, 178 and 84 absorption lines identified in the spectra of IRAS 05338 - 3051, IRAS 17279 - 1119, IRAS 18025 - 3906, IRAS 18386 - 1253 and IRAS 20259 + 4206 respectively. For this purpose we use the task ABFIND of MOOG code (Snedden, 1973). Some lines are affected by hyperfine structure (HFs) e.g. Sc, Mn, Cu, Eu, therefore in these cases, the corresponding spectral regions have been synthesized using the SPECTRUM code. For IRAS 02528 + 4350 the lines were so broad and the spectrum poor that the chemical abundances were determined exclusively from spectral synthesis.

The chemical abundances derived for the program stars are presented in Tables 3 and 4.

These tables identify the chemical species, the solar abundance from Asplund et al. (2009), the ratio of the abundances relative to hydrogen, the total uncertainty in the determination of abundances from the atmospheric model, the number of lines used or synthesized for each element, and abundances relative to iron.

**Table 2** Adopted atmospheric parameters for all stars.

No. IRAS	$T_{\text{eff}}$ (K)	$\log g$	$\xi_t$ (km s <sup>-1</sup> )	[Fe/H]	$V_r(\text{hel})$ (km s <sup>-1</sup> )	$V_r(\text{lsr})$ (km s <sup>-1</sup> )	Date
02528 + 4350	7900	2.40	2.00	-0.90	-0.9	-2.4	October 20, 2016
05338 - 3051	4250	1.50	2.50	-1.32	+5.2	-14.7	February 10, 2017
17279 - 1119	7250	1.25	4.40	-0.59	+61.6	+76.4	April 26, 2016
18025 - 3906	6250	0.25	4.00	-0.50	-120.2	-113.0	September 30, 1998
18386 - 1253	5600	0.00	4.30	-0.18	+83.2	+97.6	July 29, 2009
20259 + 4206	6100	2.20	2.36	-0.17	-15.6	+1.4	June 24, 2014

**Table 3** Elemental abundances for IRAS 02528 + 4350, IRAS 05338 - 3051 and IRAS 17279 + 1119.

Species	$\log \epsilon_{\odot}$	IRAS 02528 + 4350			IRAS 05338 - 3051			IRAS 17279 - 1119		
		[X/H]	N	[X/Fe]	[X/H]	N	[X/Fe]	[X/H]	N	[X/Fe]
C I	8.43	-0.13±0.10	syn(2)	+0.77				-0.18±0.12	7	-0.41
C (C <sub>2</sub> /CH)	8.43				-1.13±0.10	syn(4)	+0.19			
N I	7.83							+0.17±0.20	2	+0.76
N (CN)	7.83				-0.63±0.10	syn(1)	+0.69			
O I	8.69	-0.09±0.20	syn(3)	+0.81	-0.48±0.06	3	+0.84	-0.36±0.03	3	+0.23
Na I	6.24	-0.11±0.20	syn(1)	+0.79	-1.47±0.07	4	-0.15	+0.03±0.06	3	+0.56
Mg I	7.60	-0.82±0.20	syn(2)	+0.08	-0.90±0.10	4	+0.37	-0.41±0.11	2	+0.18
Mg II	7.60	-0.82±0.20	syn(1)	+0.08						
Al I	6.45				-1.53±0.03	2	-0.21			
Si I	7.51	-0.71±0.20	syn(2)	+0.19	-0.72±0.04	2	+0.60	-0.16±0.03	1	+0.43
Si II	7.51							-0.12±0.22	2	+0.47
S I	7.12							-0.02±0.00	1	+0.57
Ca I	6.34	-0.58±0.20	syn(1)	+0.32	-1.19±0.11	12	+0.13	-0.45±0.08	7	+0.13
Ca II	6.34							-0.51±0.04	1	+0.08
Sc I	3.15				-1.29±0.08	1	+0.00			
Sc II	3.15				-1.21±0.08	5	+0.11	-0.35±0.10	9	+0.24
Ti I	4.95				-1.06±0.10	9	+0.26			
Ti II	4.95	-0.95±0.20	syn(2)	-0.05	-1.12±0.08	3	+0.20	-0.11±0.12	13	+0.48
V I	3.93				-0.86±0.09	8	+0.46			
V II	3.93							-0.27±0.08	1	+0.32
Cr I	5.64	-0.97±0.20	syn(1)	-0.07	-1.15±0.07	5	+0.17	-0.31±0.04	1	+0.28
Cr II	5.64	-0.97±0.20	syn(1)	-0.07	-1.04±0.10	1	+0.28	-0.25±0.10	11	+0.33
Mn I	5.43				-1.49±0.09	2	-0.17	-1.18±0.10	3	-0.59
Fe I	7.50	-0.90±0.20	syn(4)		-1.34±0.09	37		-0.63±0.20	36	
Fe II	7.50	-0.90±0.20	syn(4)		-1.30±0.08	6		-0.54±0.14	20	
Co I	4.99				-1.24±0.09	3	+0.08			
Ni I	6.22				-0.97±0.02	5	+0.35	-0.15±0.13	2	+0.44
Ni II	6.22							-0.28±0.04	1	+0.31
Cu I	4.19				-1.48±0.10	syn(1)	-0.16			
Zn I	4.56				-1.59±0.08	2	-0.27	-0.10±0.05	1	+0.49
Sr II	2.87	-0.97±0.20	syn(2)	-0.07						
Y II	2.21				-1.02±0.05	3	+0.30	+0.41±0.09	6	+1.00
Zr II	2.58				-0.57±0.02	3	+0.75	+0.24±0.12	2	+0.82
Mo I	1.88				-0.77±0.06	2	+0.55			
Ba II	2.18	-1.08±0.20	syn(1)	-0.18	-1.13±0.07	1	+0.19	+0.32±0.20	1	+0.91
La II	1.10				-0.83±0.02	2	+0.49	+0.51±0.17	2	+1.09
Ce II	1.58				-0.93±0.09	3	+0.39	+0.38±0.09	3	+0.97
Pr II	0.72				-0.57±0.10	syn(3)	+0.75	+0.54±0.12	5	+1.12
Nd II	1.42				-0.83±0.04	8	+0.49	+0.40±0.04	2	+0.99
Sm II	0.96				-0.55±0.00	2	+0.77	+0.15±0.09	2	+0.74
Eu II	0.52				-0.43±0.12	2	+0.89	+0.17±0.05	1	+0.76
Gd II	1.07				-0.89±0.04	1	+0.53			

The abundances of the elements in Tables 3 and 4 are in a logarithmic scale with respect to hydrogen, namely:  $\log \epsilon(X) = \log [N(X)/N(H)] + 12.0$ . The abundances of the elements relative to hydrogen and iron are expressed as  $[X/H] = \log \epsilon(X)_{\text{star}} - \log \epsilon(X)_{\text{sun}}$  and  $[X/Fe] = [X/H] - [Fe/H]$  respectively.

## 5.1 Uncertainties in the elemental abundances

In this work the atomic data as the harmonic oscillator strength  $\log gf$  and low excitation potential  $\chi$  (eV) were collected from different sources, e.g. S. S. Rao et al. (2012) and references therein. The errors in the atomic data vary from element to element, for example the accuracy of experimental values for Fe I and Fe II may be between 5% and 10%. For other Fe-peak elements, errors in their  $\log gf$  may

**Table 4** Elemental abundances for IRAS 18025 - 3906, IRAS 18386 - 1253 and IRAS 20259 + 4206.

Species	log $\epsilon_{\odot}$	IRAS 18025 - 3906			IRAS 18386 - 1253			IRAS 20259 + 4206		
		[X/H]	N	[X/Fe]	[X/H]	N	[X/Fe]	[X/H]	N	[X/Fe]
C I	8.43	-0.04±0.16	20	+0.46	+0.20±0.97	12	+0.39	-0.67±0.03	2	-0.50
N I	7.83	+0.23±0.18	3	+0.74	+0.66±0.12	3	+0.84			
O I	8.69	+0.06±0.10	syn(3)	+0.56	-0.21±0.01	2	-0.03			
Na I	6.24	-0.09±0.04	4	+0.41	+0.33±0.04	1	+0.51	+0.03±0.08	2	+0.20
Mg I	7.60	-0.32±0.09	3	+0.19	+0.01±0.11	2	+0.19	-0.36±0.00	2	-0.19
Mg II	7.60	-0.06±0.09	1	+0.44						
Al I	6.45						-0.38±0.20	2	-0.22	
Si I	7.51	+0.01±0.14	14	+0.52	-0.00±0.16	11	+0.18	+0.09±0.14	4	+0.26
Si II	7.51	-0.17±0.08	2	+0.33				+0.21±0.09	2	+0.37
S I	7.12	+0.38±0.09	6	+0.88	+0.20±0.10	syn(3)	+0.38	-0.10±0.10	syn(1)	-0.07
Ca I	6.34	-0.48±0.14	13	+0.02	-0.48±0.10	10	-0.30	+0.02±0.06	4	+0.18
Ca II	6.34	-0.45±0.04	1	+0.05						
Sc II	3.15	-1.15±0.10	syn(1)	-0.65	-1.03±0.03	2	-0.85	-0.79±0.12	2	-0.62
Ti I	4.95				-0.73±0.07	2	-0.55	-0.29±0.15	4	-0.13
Ti II	4.95	-0.48±0.10	6	+0.02	-0.76±0.06	1	-0.58	-0.28±0.13	3	-0.11
V I	3.93				-0.59±0.07	2	-0.41	+0.16±0.02	1	+0.33
V II	3.93	-0.50±0.07	2	-0.00	-0.58±0.10	2	-0.40			
Cr I	5.64	-0.60±0.07	7	-0.09	-0.46±0.05	5	-0.28	-0.37±0.10	4	-0.20
Cr II	5.64	-0.39±0.14	9	+0.11	-0.72±0.15	2	-0.54	-0.39±0.08	4	-0.23
Mn I	5.43	-0.73±0.09	syn(1)	-0.23	-0.73±0.15	3	-0.55	-0.67±0.13	2	-0.51
Fe I	7.50	-0.50±0.12	56		-0.19±0.11	61		-0.17±0.11	19	
Fe II	7.50	-0.51±0.17	18		-0.17±0.11	12		-0.07±0.06	5	
Co I	4.99				-0.60±0.08	1	-0.42	+0.12±0.04	2	+0.29
Ni I	6.22	-0.43±0.12	13	+0.08	-0.33±0.15	14	-0.15	-0.44±0.08	6	-0.28
Ni II	6.22	-0.56±0.04	1	-0.06						
Cu I	4.19	-0.38±0.04	1	+0.13	-0.37±0.20	syn(1)	-0.19	-0.33±0.04	1	-0.16
Zn I	4.56	-0.33±0.12	4	+0.18	-0.21±0.19	2	-0.02	-0.11±0.06	2	-0.06
Y II	2.21	-1.31±0.16	3	-0.80	-1.25±0.11	3	-1.07	-0.64±0.01	2	-0.48
Zr II	2.58	-1.35±0.04	1	-0.84	-0.59±0.04	1	-0.41	-1.32±0.01	1	-1.15
Ba II	2.18	-0.52±0.07	1	-0.01				-0.71±0.15	3	-0.54
La II	1.10				-0.88±0.05	1	-0.70	+0.01±0.05	1	+0.18
Ce II	1.58	-0.92±0.07	1	-0.41	-1.09±0.09	4	-0.91			
Nd II	1.42	-0.42±0.19	2	+0.09	-1.24±0.04	1	-1.06			
Sm II	0.96	-0.63±0.06	1	-0.12	-1.22±0.10	2	-1.04	-0.23±0.06	1	-0.06
Eu II	0.52	-0.33±0.06	1	+0.18	-0.33±0.10	syn(1)	-0.15			

range between 10% and 25%, while for neutron-capture elements the precision is about 10%.

In order to estimate the uncertainties in the resulting elemental abundances, we calculated the effect of varying temperature, gravity and turbulent velocity within the ranges  $\pm 250\text{K}$ ,  $\pm 0.25$  dex and  $\pm 0.5$   $\text{kms}^{-1}$  respectively. The sensitivity of the derived abundances to these changes in the model atmosphere input parameters is exemplified in Table 5. The errors due to equivalent widths are random ( $\sigma_{ran}$ ) since they depend on several factors such as the position of the continuum, the signal-to-noise (S/N) ratio and spectral type of the star. In contrast, the errors due to the atmospheric parameters and atomic data are systematic ( $\sigma_{sys}$ ) and depend on the precision with which we have been able to estimate them.

The total error  $\sigma_{tot}$  for each element can be estimated through the square root of the quadratic sum of the random and systematic errors (see Table 5).

## 6 INDIVIDUAL ABUNDANCES

### 6.1 IRAS 02528 + 4350

The spectrum has broad and very low-intensities lines and their cores are affected by noise. We report a rotation ve-

locity of about  $55 \text{ km s}^{-1}$  and a heliocentric radial velocity of  $-0.9 \pm 0.3 \text{ km s}^{-1}$  derived from Na I D<sub>1</sub> and D<sub>2</sub> measured between two subsequent orders.

The star is moderately metal-poor and has few identified elements. CNO abundances are based upon the synthesis of two C lines ( $\lambda 5052\text{\AA}$  and  $\lambda 5830\text{\AA}$ ) and the O I triplet at  $\lambda 6150\text{\AA}$ . We derive a moderate enrichment LTE value of carbon [C/H] of  $-0.13$  and [C/Fe] of  $+0.77$ , while the oxygen shows a similar enrichment to that of carbon, [O/H] =  $-0.09$  and [O/Fe] =  $+0.81$  respectively. Non-LTE corrections of  $-0.39$ ,  $-0.17$  and  $\sim 0.25$  for C, O and Fe were taken from Venn (1995), Takeda & Takada-Hidai (1998) and Lind et al. (2012) leading to values of [C/Fe] =  $+0.13$  and [O/Fe] =  $+0.39$ . The non-LTE corrected values of carbon and oxygen abundances indicate a C/O ratio slightly lower than the solar value (C/O  $\sim 0.5$ ), i.e.  $+0.3$ .

The Na abundance is derived from the line at  $\lambda 6160$  and shows a moderate enhancement, [Na/Fe] =  $+0.79$ . A non-LTE correction of  $-0.10$  taken from Lind et al. (2011) leads to a value of [Na/Fe] =  $+0.44$  which indicates that such enrichment is real and is possibly caused by proton capture on  $^{22}\text{Ne}$  in H-burning region. The behaviour of  $\alpha$ -elements ([ $\alpha$ /Fe] =  $+0.14$ ) is not fully compatible with the thick disc values, in fact, [Ca/Fe] =  $+0.32$  shows a value typical of thick disc stars but [Mg/Fe] =  $+0.08$ , [Si/Fe] =  $+0.19$  and



**Table 5** Sensitivity of abundances to the uncertainties in the model parameters for a range of temperature covering our sample stars.

Species	IRAS 05338 - 3051 (4250K)				IRAS 18386 - 1253 (5600K)				IRAS 18025 - 3906 (6250K)			
	$\Delta T_{\text{eff}}$ +250	$\Delta \log g$ +0.25	$\Delta \xi_r$ +0.50	$\sigma_{\text{tot}}$	$\Delta T_{\text{eff}}$ +250	$\Delta \log g$ +0.25	$\Delta \xi_r$ +0.50	$\sigma_{\text{tot}}$	$\Delta T_{\text{eff}}$ +250	$\Delta \log g$ +0.25	$\Delta \xi_r$ +0.50	$\sigma_{\text{tot}}$
C I					+0.07	-0.06	+0.03	0.09	-0.04	-0.02	+0.03	0.05
N I					+0.18	-0.08	+0.05	0.20	+0.10	-0.05	+0.03	0.12
O I	-0.12	+0.10	+0.02	0.16	-0.09	-0.06	+0.01	0.10	+0.02	-0.05	+0.03	0.06
Na I	-0.21	-0.04	+0.05	0.22	-0.12	+0.03	+0.02	0.13	-0.17	+0.05	+0.02	0.18
Mg I	-0.16	-0.02	+0.06	0.17	-0.09	+0.02	+0.07	0.12	-0.15	+0.04	+0.04	0.16
Mg II									+0.08	-0.05	+0.07	0.12
Si I	+0.01	+0.07	+0.01	0.07	-0.11	+0.03	+0.02	0.11	-0.17	+0.05	+0.02	0.17
Si II									+0.09	-0.05	+0.02	0.11
S I					+0.01	-0.04	+0.07	0.08	-0.11	+0.01	+0.03	0.12
Ca I	-0.28	-0.04	+0.18	0.31	-0.15	+0.03	+0.04	0.16	-0.23	+0.05	+0.04	0.24
Ca II									-0.02	-0.06	+0.06	0.08
Sc II	-0.25	-0.00	+0.01	0.25	-0.07	-0.07	+0.07	0.12	-0.14	-0.06	+0.06	0.16
Ti I	-0.30	-0.04	+0.08	0.31	-0.22	+0.04	+0.01					
Ti II	-0.06	-0.17	+0.17	0.25	-0.08	-0.06	+0.09	0.13	-0.12	-0.06	+0.08	0.16
V I	-0.30	-0.00	+0.08	0.31	-0.23	+0.04	+0.01					
V II					-0.05	-0.06	+0.01	0.08	-0.11	-0.06	+0.03	0.13
Cr I	-0.23	-0.03	+0.07	0.24	-0.20	+0.04	+0.05	0.21	-0.24	+0.04	+0.02	0.25
Cr II	+0.10	+0.18	+0.02	0.21	-0.06	-0.06	+0.06	0.10	-0.06	-0.06	+0.06	0.10
Mn I	-0.29	-0.01	+0.12	0.32	-0.17	-0.00	+0.01	0.17	-0.22	+0.04	+0.01	0.23
Fe I	-0.22	+0.01	+0.10	0.24	-0.16	+0.03	+0.05	0.17	-0.22	+0.04	+0.03	0.22
Fe II	+0.13	+0.13	+0.07	0.19	-0.01	-0.07	+0.08	0.11	-0.07	-0.06	+0.05	0.10
Co I	-0.20	+0.05	+0.02	0.21	-0.17	+0.04	+0.01					
Ni I	-0.25	+0.07	+0.17	0.31	-0.16	+0.03	+0.07	0.17	-0.22	+0.04	+0.01	0.22
Ni II									-0.06	-0.06	+0.03	0.09
Cu I					-0.20	+0.04	+0.04	0.21	-0.26	+0.05	+0.02	0.27
Zn I	+0.05	+0.12	+0.06	0.15	-0.16	+0.03	+0.05	0.17	-0.22	+0.04	+0.02	0.22
Y II	-0.09	+0.17	+0.14	0.24	-0.09	-0.06	+0.03	0.11	-0.16	-0.05	+0.01	0.17
Zr I	-0.28	+0.01	+0.04	0.29								
Zr II					-0.10	-0.06	+0.13	0.17	-0.13	-0.06	+0.00	0.14
Mo I	-0.21	-0.02	+0.01	0.21								
Ba II	-0.21	+0.18	+0.16	0.32					-0.21	+0.01	+0.12	0.24
La II	-0.16	+0.10	+0.03	0.19	-0.13	-0.06	+0.09					
Ce II	-0.11	+0.19	+0.02	0.22	-0.13	-0.05	+0.02	0.14	-0.22	-0.04	+0.01	0.22
Nd II	-0.15	+0.18	+0.06	0.25	-0.15	-0.05	+0.04	0.16	-0.27	-0.02	+0.01	0.27
Sm II	-0.15	+0.17	+0.07	0.24	-0.13	-0.05	+0.01	0.14	-0.24	-0.04	+0.00	0.24
Eu II	-0.08	-0.02	+0.03	0.09	-0.10	-0.06	+0.10	0.16	-0.20	-0.04	-0.19	0.28
Gd II	-0.13	+0.12	+0.03									

$[\text{Ti}/\text{Fe}] = -0.05$  are lower than expected to thick disc population. On the other hand, the Cr, Sr and Ba abundances  $[\text{X}/\text{H}]$  show depletion, and unfortunately S and Zn elements are not present to corroborate this effect. In addition, Mg, Si and Cr do not show the trend of dust-gas winnowing (DG-effect).

## 6.2 IRAS 05338 - 3051

IRAS 05338 - 3051 is a semi-regular variable with a pulsation period of 105.7 days and  $V$  light variations between 9.30 and 10.30 mag (Kukarkin et al., 1971; Samus et al., 2009).

The heliocentric radial velocity of the star measured from the spectrum taken on Feb 10, 2017 was of  $+5.2 \pm 0.5$   $\text{kms}^{-1}$ . The spectrum of the star is not crowded but contains a large number of lines for several important elements. The star is metal-deficient with  $[\text{Fe}/\text{H}] = -1.3$  dex. The high galactic latitude of IRAS 05338 - 3051 combined with its low metallicity indicates that the star probably belongs to the old-disk population of the Galaxy.

In view of the fact that our object is cooler than the Sun, we use the Arcturus spectrum as a reference to calibrate

our line list of the identified EWs. The condition for verifying the quality of our line list requires that the abundances obtained agree satisfactorily with those estimated in other works. By comparing our abundances with those obtained by Ramírez & Allende Prieto (2011), we noted no systematic differences greater than 0.03 dex. The elemental abundances of IRAS 05338 - 3051 are presented in Table 3.

IRAS 05338 - 3051 does not show sodium enrichment ( $[\text{Na}/\text{Fe}] = -0.15$  dex). A moderate enrichment of the  $\alpha$  elements (Mg, Si, Ca, Ti) of +0.33 dex has been observed, typical of the thick disc population. Magnesium ( $[\text{Mg}/\text{Fe}] = +0.37$ ) and silicon ( $[\text{Si}/\text{Fe}] = +0.60$ ) show much larger values than calcium ( $[\text{Ca}/\text{Fe}] = +0.13$ ) and titanium ( $[\text{Ti}/\text{Fe}] = +0.23$ ). Iron-peak elements (Sc, V, Cr, Ni) show  $[\text{X}/\text{Fe}]$  abundances mildly enhanced that vary from +0.05 to +0.46 dex. We observe also that the vanadium and nickel are surprisingly overabundant relative to the solar value,  $[\text{V}/\text{Fe}] = +0.46$  and  $[\text{Ni}/\text{Fe}] = +0.35$  dex.

Neutron-capture (s-and-r process) elements have  $[\text{X}/\text{Fe}]$  abundances moderately enriched. s-process elements as Y, Zr, Ba, La, Ce, Nd and Sm show abundances varying from +0.19 to +0.77 dex, while r-process elements as Pr, Eu

range from +0.75 to +0.89 dex respectively. Our analysis covers light s-process elements (ls) Y and Zr and heavy s-process elements (hs) Ba, La, Ce and Nd. We derive a mean  $[\text{ls}/\text{Fe}]$  of +0.53 dex and mean  $[\text{hs}/\text{Fe}]$  of +0.47 dex. That leads to the ratio of hs-elements to ls-elements  $[\text{hs}/\text{ls}]$  of  $-0.06$  dex.

With a moderate enrichment of s-elements one would expect that C is enriched, however, surprisingly we note that it is very deficient ( $[\text{C}/\text{H}] = -1.13$  dex). Our C abundance has been estimated by synthesizing several regions with  $\text{C}_2$  ( $\lambda 4732\text{--}4744$ ;  $\lambda 5133\text{--}5165$ ;  $\lambda 5626\text{--}5636$ ) and CH bands, ( $\lambda 4290\text{--}4310$ ). The N abundance is derived from the CN region at  $\lambda 4213\text{--}4216$ . We observe a moderate enhancement of  $[\text{N}/\text{Fe}]$  abundance of +0.69 which involves a conversion of initial C into N through the CN-cycle. The O abundance was estimated from three lines ( $\lambda 5577$ ,  $\lambda 6300$  and  $\lambda 6363$ ) and shows an enriched value of  $[\text{O}/\text{Fe}] = +0.84$  dex. The C/O ratio is about of +0.12.

Our derived abundances have the same trend observed in V453 Oph studied by Deroo et al. (2005). V453 Oph is a RV Tauri star which shows low metallicity ( $[\text{Fe}/\text{H}] \sim -2.2$  dex), s-process enrichment but C deficiency and has no infrared excess.

### 6.3 IRAS 17279-1119

IRAS 17279-1119 is a PAGB star that has been the subject of several previous abundance analysis. Van Winckel (1997) suggested that it is a pulsating variable. Bogaert (1994) identified two possible periods; 61 and 93 day, although more photometric data would be required to confirm them.

Van Winckel (1997) derived the values  $T_{\text{eff}} = 7400\text{K}$ ,  $\log g = 0.5$  and  $[\text{Fe}/\text{H}] = -0.7$  dex. From a detailed abundance analysis the star is revealed as metal-poor, with C, N moderately enriched and enriched s-process elements.

Arellano Ferro et al. (2001) estimated  $T_{\text{eff}} = 7300\text{K}$ ,  $\log g = 1.5$ ,  $\xi_t = 4.6 \text{ km s}^{-1}$  and  $[\text{Fe}/\text{H}] = -0.6$  dex. They also found that the star is metal-poor, and have a moderate enrichment in C, Na, Sc and s-process elements. In agreement with the above results S. S. Rao et al. (2012) estimated  $T_{\text{eff}} = 7250\text{K}$ ,  $\log g = 2.25$ ,  $\xi_t = 4.7 \text{ km s}^{-1}$  and  $[\text{Fe}/\text{H}] = -0.43$  dex.

We note that the metallicity estimated by S. S. Rao et al. (2012) is slightly higher than those obtained by Van Winckel (1997) and Arellano Ferro et al. (2001). The present N abundance,  $[\text{N}/\text{Fe}] = -0.3$  dex, is higher than that obtained by Van Winckel (1997) ( $[\text{N}/\text{Fe}] = -0.6$  dex). C and s-process abundances are moderately enriched (see Table 8).

A recent abundance analysis was carried out by De Smedt et al. (2016). Their derived atmospheric parameters were  $T_{\text{eff}} = 7250\text{K}$ ,  $\log g = 1.25$ ,  $\xi_t = 3.0 \text{ km s}^{-1}$  and  $[\text{Fe}/\text{H}] = -0.64$  dex. According to these authors, IRAS 17279-1119 has a moderate C enhancement, displays a mild s-process enrichment and most of the s-process

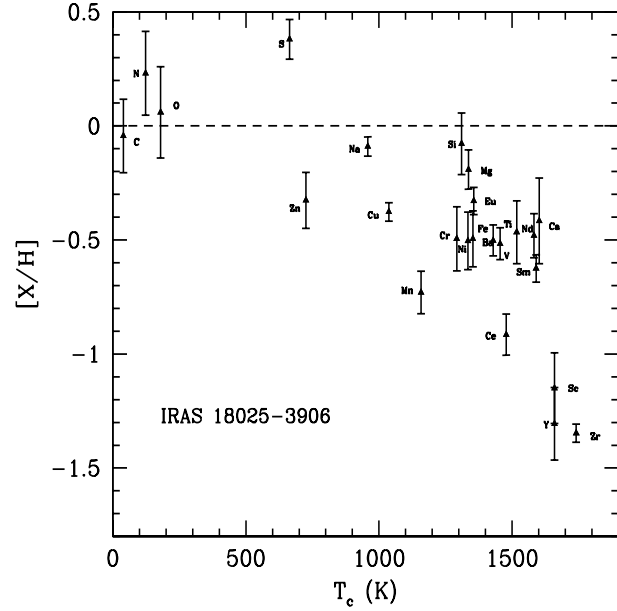


**Fig. 5** Abundance  $[\text{X}/\text{H}]$  versus condensation temperature  $T_c$  for IRAS 18025-3906.

elements have an  $[\text{X}/\text{Fe}] < 1.0$  dex. Their calculation of  $[\text{N}/\text{Fe}] = -0.07$  dex, does not show the enhancement obtained by S. S. Rao et al. (2012), (+0.63). This object shows evidence of being moderately metal-poor and have moderately enriched abundances of s-process elements.

For IRAS 17279-1119 we have adopted the atmospheric parameters  $7250\text{K}$ ,  $1.25$ ,  $4.4 \text{ km s}^{-1}$  and  $-0.59$  dex for  $T_{\text{eff}}$ ,  $\log g$ ,  $\xi_t$  and  $[\text{Fe}/\text{H}]$  respectively (see Table 2). We have determined the carbon, nitrogen and oxygen abundances for this object based upon a fairly large number of lines. The abundances  $[\text{C}/\text{H}]$  and  $[\text{C}/\text{Fe}]$  of  $-0.18$  and  $+0.41$ ,  $[\text{N}/\text{H}]$  and  $[\text{N}/\text{Fe}]$  of  $+0.17$  and  $+0.76$  and  $[\text{O}/\text{H}]$  and  $[\text{O}/\text{Fe}]$  of  $-0.36$  and  $+0.23$  were found. At this temperature, the non-LTE corrections are  $-0.17$ ,  $-0.30$  and  $-0.10$  for C, N and O respectively and imply  $[\text{C}/\text{Fe}]$  of  $+0.10$ ,  $[\text{N}/\text{Fe}]$  of  $+0.30$  and  $[\text{O}/\text{Fe}]$  of  $-0.03$ . The moderate N enrichment, implying conversion of initial carbon into N through CN-cycle, and the observed near-solar O abundance, does not indicate ON processing. The C/O ratio is about 0.82 dex.

IRAS 17279-1119 shows relative enrichment of sodium possibly caused by proton capture on  $^{22}\text{Ne}$ . The  $\alpha$ -elements display a consistent enrichment relative to Fe of +0.3 dex typical for the thick disc stars. The Fe-peak elements  $[\text{Ni}/\text{Fe}]$  and  $[\text{Zn}/\text{Fe}]$  show a moderate enrichment of +0.38 and +0.49 dex respectively. s-process elements exhibit a mild enhancement observed previously by Van Winckel (1997), Arellano Ferro et al. (2001), S. S. Rao et al. (2012) and De Smedt et al. (2016). We estimated the heavy s-process  $[\text{hs}/\text{Fe}] = +0.94$  and the light s-process  $[\text{ls}/\text{Fe}] = +0.91$  while the  $[\text{hs}/\text{ls}]$  ratio is  $\sim 0.03$ . The abundances of IRAS 17279-1119 are given in Table 3.

Our abundances are in agreement, on average within  $\pm 0.2$  dex, with those derived by De Smedt et al. (2016) with

the exception of nitrogen and manganese. Our N abundance ( $[N/Fe] = +0.76$  dex) however has a similar value to that obtained by S. S. Rao et al. (2012) of  $[N/Fe] = +0.63$  dex, while Mn abundance is very deficient,  $[Mn/Fe] = -0.59$  dex. Manganese deficiency is difficult to explain. According to De Smedt et al. (2016), IRAS 17279 - 1119 is the first s-process rich PAGBs discovered to be in a spectroscopic binary and the precursor of extrinsically s-process enriched stars.

#### 6.4 IRAS 18025 - 3906

IRAS 18025 - 3906 (GLMP 713) has been classified as G2 by Hu et al. (1993). The heliocentric radial velocity from 86 lines in the spectrum taken on September 30, 1998 is  $-120.2 \pm 0.6$   $\text{km s}^{-1}$ . Our value of LSR velocity ( $-113.0$   $\text{km s}^{-1}$ ) is very similar that obtained by Silva et al. (1993) of  $-116.0$   $\text{km s}^{-1}$ . The photospheric abundances of IRAS 18025 - 3906 show a moderate metal-deficiency ( $[Fe/H] = -0.50$  dex). This star exhibits a large number of C I lines ( $\sim 20$  lines). The N abundance appears enriched by the CN process ( $[N/Fe] = +0.74$ ), while  $[C/Fe] = +0.46$  points to the products of He burning being brought to the surface. The  $[O/Fe]$  of  $+0.56$  is slightly larger than  $[C/Fe]$  but the C/O ratio is  $\sim 0.43$ . The Na abundance has a moderate enrichment probably caused by proton capture on  $^{22}\text{Ne}$  ( $[Na/Fe] = +0.41$ ). A  $[\alpha/Fe] = +0.22$  ratio and the high radial velocity, are similar to the observed in objects of the thick disk. Individually, S is enriched ( $[S/Fe] = +0.88$ ), whereas the Mg and Si have a moderate enrichment ( $[Mg/Fe] = +0.31$  and  $[Si/Fe] = +0.43$ ). The Zn abundance is nearly solar ( $[Zn/Fe] = +0.18$ ). Fe-peak abundances  $[X/Fe]$  varying between  $-0.65$  to  $+0.01$ , while the s-process elements range from  $-0.84$  to  $+0.18$ . We have plotted in Fig. 5 the observed abundances for IRAS 18025 - 3906 as function of the condensation temperature for the elements (Lodders, 2003). From the relations  $[X/H]$  versus  $T_c$  we noted that IRAS 18025 - 3906 shows a modest depletion.

To verify if this object actually presents depletion, we calculated the abundances of photospheric depletion traces, such as  $[Zn/Ti]$  and  $[S/Ti]$  respectively. For IRAS 18025 - 3906 we found  $[Zn/Ti] = +0.15$  and  $[S/Ti] = +0.86$ , showing that this object is not depleted. In addition, its SED has shell-type structure (Hu et al., 1993) suggesting the presence of cold dust away from the central star and its non-binary nature. There is observational evidence that PAGBs with a C/O  $< 1$  ratio are rich in oxygen and do not exhibit s-process enrichment, which suggests that the TDU has not been efficient in the AGB phase. The C/O  $\sim 0.43$  and the non-enrichment of s-process elements could point that IRAS 18025 - 3906 is probably a PAGB with this type of peculiarities.

However, one of the problems that difficult to predict the PAGB stage for optically visible galactic PAGBs is that their distances and luminosities are unknown. Gaia DR2 source provides parallaxes for a  $\sim 1.7$  billion of stars in the Milky Way, although not all the stars present in this source have

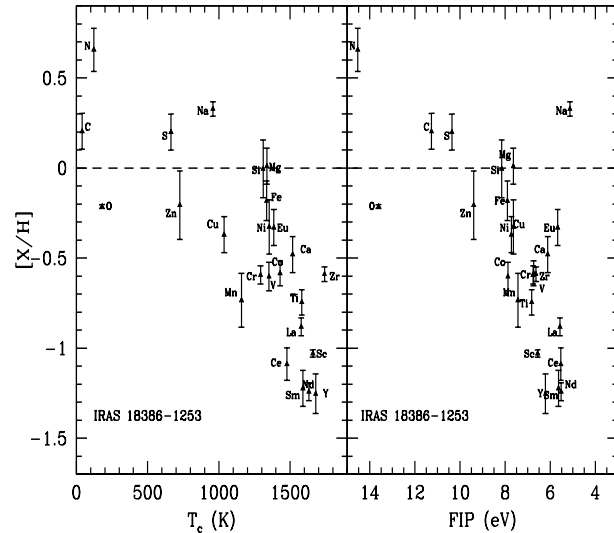


**Fig. 6** Abundance  $[X/H]$  versus condensation temperature  $T_c$  (left panel) and first ionization potential FIP (right panel) for IRAS 18386 - 1253.

a precise parallaxes ( $\sigma_p/p \lesssim 20\%$ ). For some stars with distances greater than 4 kpc from the Sun, the relative error could exceed 25%. We can observe that the parallax for IRAS 18025 - 3906 has a very large relative error, close to 99% ( $p = 0.4399 \pm 0.4387$  mas). Vickers et al. (2015) assume a luminosity of  $6000 \pm 1500 L_\odot$  for this object, and indicate that it belongs to the intermediate thin disk with ranges in age, metallicity and mass of 0.7–3.0 Gyr,  $-0.2$  to  $+0.5$  and  $1.6$ – $3.0 L_\odot$ . However, we can see that our metallicity is lower than the proposed range for this population ( $-0.50$  dex), this would lead us to deduce that IRAS 18025 - 3906 rather belongs to the old thin disk population with a luminosity of  $3500 \pm 1500 L_\odot$  (see Table 3 in Vickers et al. (2015)).

#### 6.5 IRAS 18386 - 1253

This PAGB candidate was analysed by Pereira & Miranda (2007) with low-resolution spectra and classified it as a probable F5 type star. The heliocentric radial velocity obtained from 115 lines in the spectrum taken on July 29, 2009 is  $+83.2 \pm 0.5$   $\text{km s}^{-1}$ . The star shows a marginal iron deficiency,  $[Fe/H] = -0.18$  dex.

The C abundance  $[C/Fe] = +0.39$  dex, derived from a large number of lines shows a moderate enrichment and  $[N/Fe] = +0.84$  dex indicates strong signatures of the CN cycle. The  $[O I]$  forbidden lines  $\lambda 5577\text{\AA}$  and  $\lambda 6363\text{\AA}$  lead to  $[O/Fe] = -0.03$ . IRAS 18386 - 1253 is C-rich since the C/O ratio is slightly greater than one (C/O  $\sim 1.4$ ). The s-process elements do not display any enrichment.  $[\alpha/Fe] = +0.25$  shows a consistent enrichment relative to Fe expected for the thick disk population but with a low metallicity. The photospheric depletion tracers  $[Zn/Ti] = +0.54$  and  $[S/Ti] = +0.95$  indicate that IRAS 18386 - 1253 is mildly depleted.

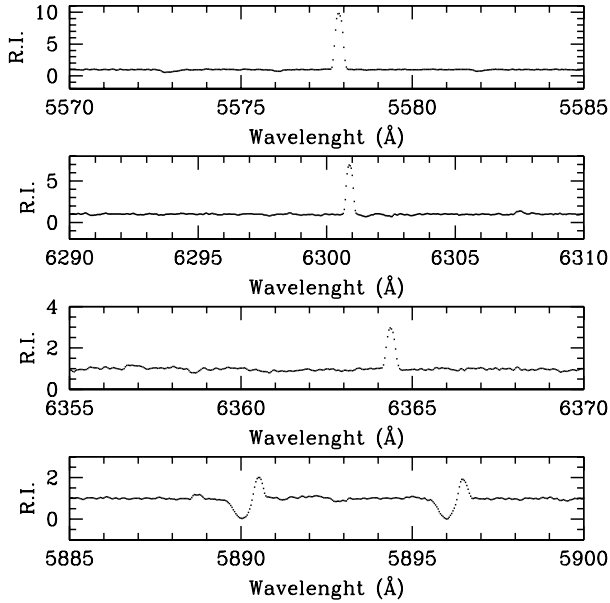


**Fig. 7** Emissions present in the forbidden oxygen lines at  $\lambda 5577\text{\AA}$ ,  $\lambda 6300\text{\AA}$  and  $\lambda 6364\text{\AA}$  and Na I D doublet for IRAS 20259 + 4206.

It is tempting to ascribe this depletion only to dust condensation, however the large scatter observed may suggest that another mechanism operates simultaneously. This other mechanism might be the first ionization potential (FIP) effect initially seen in the solar chromosphere and corona where ions of low-FIP elements rather than neutral atoms are fed from the chromosphere to the corona. In this sense the plot  $[X/H]$  versus FIP in Fig. 6 shows that there is a good correlation between the high-FIP and low-FIP elements with the exception of O and Na for IRAS 18386 - 1253. This phenomenon was observed by N. K. Rao & Reddy (2005) for the two RV Tauri stars CE Vir and EQ Cas. These authors propose that singly ionized elements escaped as stellar wind rather than being coupled to the radiation pressure on the dust.

It is clear that elements with a FIP of 8 eV or lower show systematic depletion. This phenomenon has also been observed in the stars CpD - 62 5428 (Giridhar et al., 2010) and IRAS 18321 - 1401 (Molina et al., 2014). The smooth anticorrelation between the abundances and the FIP effect suggests that the removed elements systematically correspond to species with the first ionized states.

García-Segura et al. (2005) suggest that magnetic field driven winds have the potential to remove ionized elements in the photosphere of PAGB stars although the existence of stellar winds must be verified for IRAS 18386 - 1253. The mechanism that provides the overionization, however, is not entirely understood. A multi-wavelength monitoring of this star IRAS 18386 - 1253 may be required to understand its peculiar abundance patterns.

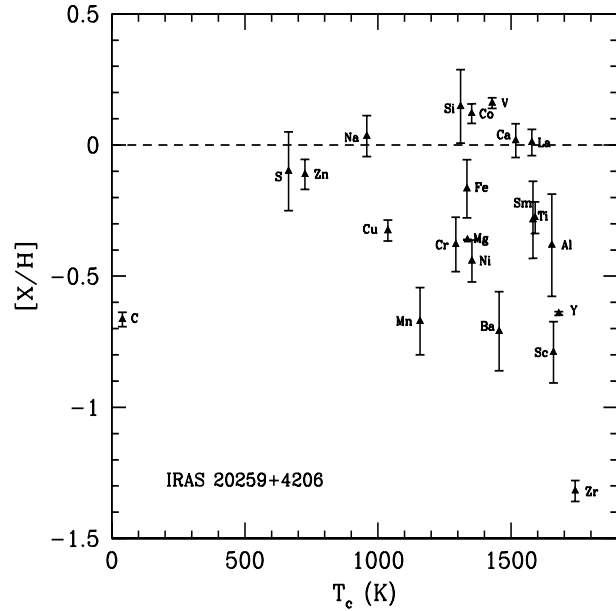


**Fig. 8** Abundance  $[X/H]$  versus condensation temperature  $T_c$  for IRAS 20259 + 4206.

## 6.6 IRAS 20259 + 4206

The present abundance analysis of IRAS 20259 + 4206 is the first performed for this star. For this object a heliocentric radial velocity of  $-15.6 \pm 0.6 \text{ km s}^{-1}$  was measured using 125 lines. The adopted model atmosphere parameters are given in the Table 2 and the resulting abundances are listed in Table 4. The profiles of the Na I D lines show emission in the right wings, suggesting that this object undergoes a strong mass-loss (see Fig. 7).

The star is slightly metal poor ( $[Fe/H] = -0.17$  dex). It also shows an under abundance of carbon ( $[C/H] = -0.64$ ) obtained from two lines;  $\lambda 6587.6\text{\AA}$  and  $\lambda 5380.3\text{\AA}$ . Due to our limitation in the spectral range we can not measure the abundance of N, therefore we can not predict the CN-cycle efficiency. We also can not measure the O abundance. The O I triplet lines at  $\lambda 6155\text{--}60\text{\AA}$  are contaminated while the forbidden lines [O I]  $\lambda 5577\text{\AA}$ ,  $\lambda 6300\text{\AA}$  and  $\lambda 6364\text{\AA}$  are affected by emission (see Fig. 7). Sodium has a modest enhancement ( $[Na/Fe] = +0.20$ ). The  $[\alpha/Fe]$  ratio of  $\sim 0.06$  obtained from S, Si and Mg, is similar to those found in thin disk objects. Sulfur abundance is derived from synthesis by taking into account only the line  $\lambda 6757.1\text{\AA}$  of the triplet at  $\lambda 6743\text{--}58\text{\AA}$ . The  $\lambda 6743\text{\AA}$  and  $\lambda 6748\text{\AA}$  lines could be affected by blends. Its value is near to solar, i.e.  $[S/Fe] = 0.07$  dex.

In Fig. 8 we have plotted the observe abundances for IRAS 20259 + 4206 as function of the condensation temperature. Modest depletion patterns with great scatter are observed in certain elements with  $T_c > 1300\text{K}$ , e.g. Cr, Mg, Fe, Ti, Sm, Al, Ni, Ba, Sc and Y, while Zr is more depleted by at least one order of magnitude. Other elements such as Si, Ca, V, Co, La do not show depletion. The low signal-to-

noise ( $S/N \sim 30$ ), the moderate resolution and the limitation on the spectral range make necessary that this object is analyzed with more favourable data.

## 7 Discussion

In the sample of PAGB candidate stars in the present study, there are five objects not previously studied spectroscopically; IRAS 02528 + 4350, IRAS 05338 - 3051, IRAS 18326 - 1253, IRAS 18025 - 3906, and IRAS 20259 + 4206. On the other hand, the elemental abundances of the star IRAS 17279 - 1119, have been calculated by several investigators (Arellano Ferro et al., 2001; De Smedt et al., 2016; S. S. Rao et al., 2012; Van Winckel, 1997). An exhaustive abundance analysis is carried out to discriminate among the enormous chemical variety that these kind of objects may exhibit.

In the majority of the sample stars we find evidence of CN processing, with the exception of IRAS 02528 + 4350 and IRAS 20259 + 4206, in which it was not possible to determine the N abundance. In the remaining objects, the  $[N/Fe]$  ratio ranges between +0.7 and +0.8 dex. We have also seen the signature of mixing of He-burning products via the TDUP for IRAS 02528 + 4350, IRAS 05338 - 3051, IRAS 17279 - 1119, IRAS 18025 - 3906 and IRAS 18326 - 1253. In fact, the  $[C/Fe]$  ratio ranges from +0.10 to +0.46 dex. IRAS 20259 + 4206, clearly exhibits an underabundance of carbon of  $-0.50$  dex. This deficiency of C is greater than that caused by the CN-cycle, which leads to a N enhancement. A possible alternative to the observed carbon reduction could point out towards a Hot Bottom Burning (HBB) phenomenon, that operates in AGB stars more massive than  $4 M_{\odot}$ , and that partially converts the C excess in the envelope into N. Unfortunately we have been unable to determine the expected Li enrichment in the case of HBB (Sackmann & Boothroyd, 1992).

### 7.1 Sodium, $\alpha$ -elements and s-process elements

For all the sample stars the  $[Na/Fe]$  abundance varies between  $-0.15$  and  $+0.79$  dex.  $[Na/Fe]$  abundance is commonly determined from lines at  $\lambda 5682\text{\AA}$ ,  $\lambda 5688\text{\AA}$ ,  $\lambda 6154\text{\AA}$  and  $\lambda 6160\text{\AA}$ . For the temperature range of our sample (i.e.  $4250\text{K}-7900\text{K}$ ), the non-LTE correction could vary between  $-0.10$  to  $-0.16$  dex (Lind et al., 2011). With this correction, the observed values are not significantly affected, which suggests that Na enrichment is real and probably comes via proton capture on  $^{22}\text{Ne}$ . Only IRAS 05338 - 3051 shows a subsolar value;  $[Na/Fe] = -0.25$  dex.

Regarding the  $\alpha$ -elements, in IRAS 18386 - 1253, the  $[\alpha/Fe]$  was obtained exclusively from Mg, Si and S because Ca and Ti could be affected by depletion and non-LTE effect. IRAS 18386 - 1253 has a value of +0.26 typical of thick-disk with metallicities nearly solar. The high radial velocity observed for this object would confirm this fact.

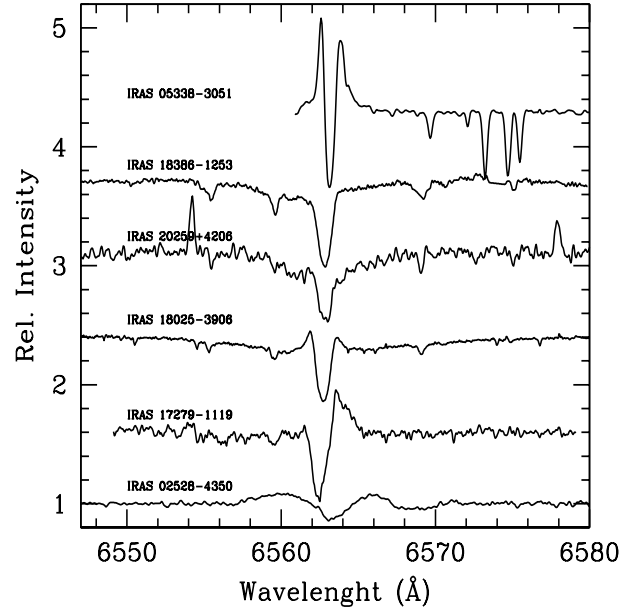


**Fig. 9** Variability of the absorption and emission  $H\alpha$  profiles for IRAS 02528 + 4350, IRAS 05338 - 3051, IRAS 17279 - 1119, IRAS 18025 - 3906, IRAS 18386 - 1253 and IRAS 20259 + 4206.

IRAS 18025 - 3906 exhibits a moderate enrichment of  $\alpha$ -elements ( $[\alpha/Fe] \sim +0.22$ ) expected for objects of the thick-disk.

On the other hand, IRAS 05338 - 3051, exhibits a moderate enrichment of  $\alpha$ -elements of +0.33 derived from Mg, Si, Ca and Ti respectively. Its low-metallicity,  $[Fe/H] = -1.3$ , points it as thick-disk or Galactic halo object. The  $[\alpha/Fe]$  for IRAS 02528 + 4350 of +0.14 and its  $[Fe/H] = -0.9$  support an unevolved object of thin-disk population. IRAS 17279 - 1119 shows a moderate enrichment of  $\alpha$ -elements of +0.33 with  $[Fe/H] = -0.6$  suggesting that it is an object of the thick-disk population. IRAS 20259 + 4206 exhibit  $[\alpha/Fe] = +0.05$  with  $[Fe/H] = -0.2$  which is typical of objects of the thin-disk.

### 7.2 $H\alpha$ and Sodium doublet profiles

The  $H\alpha$  profiles in PAGB stars are affected by instability of the dynamic processes in the extended atmosphere and its envelope. These profiles show a range in the emission-absorption structure related to the complex atmospheric motions (or perturbations) that propagate throughout the atmospheric layers.

Fig. 9 shows the  $H\alpha$  profiles of the six program stars. In IRAS 20259 + 4206 and IRAS 18386 - 1253, the  $H\alpha$  profile shows a broad shallow component and central filling with asymmetric emission. Evidently, emission is not strong enough to rise above the continuum. This emission could be produced in a circumstellar cloud of (hot) gas or an extended envelope (Arellano Ferro, 1985).

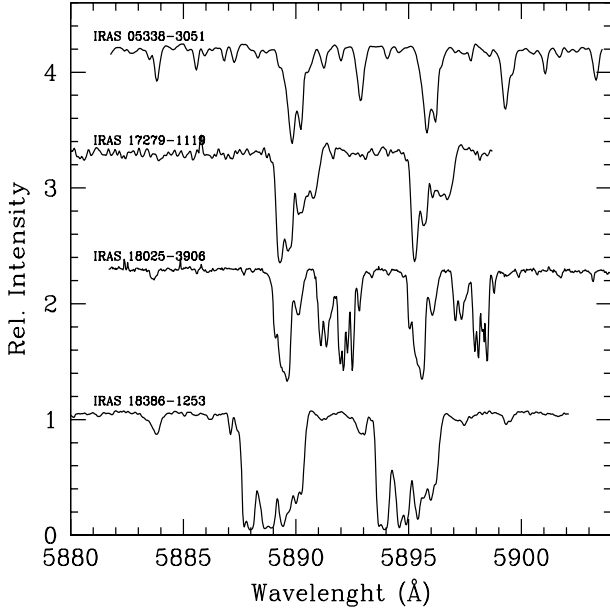


**Fig. 10** Complex structure of  $D_2$  ( $\lambda$  5890) and  $D_1$  ( $\lambda$  5895) Na I line profiles in four objects in the sample. Multi-component interstellar absorption lines are present in their spectra.

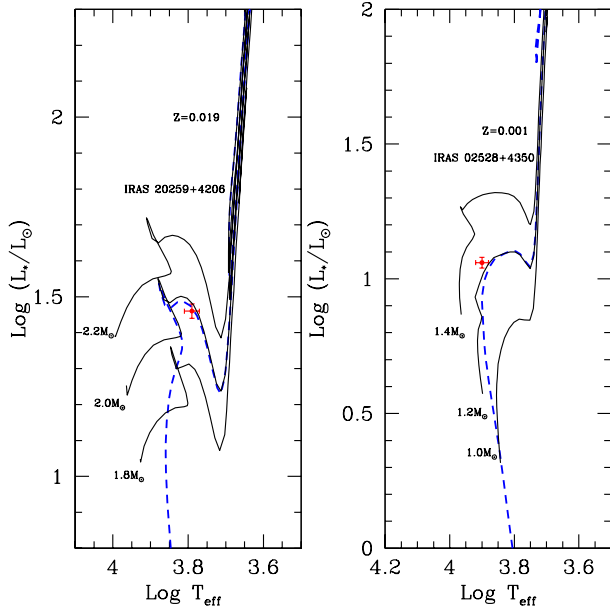


**Fig. 11** Evolutionary tracks in the HRD for two compositions [ $Z=0.019$ ,  $Y=0.273$ ] and [ $Z=0.001$ ,  $Y=0.230$ ], where  $Y$  and  $Z$  represent the helium and metal mass fractions. IRAS 02528 + 4350 is moderately iron-deficient and IRAS 20259 + 4206 shows nearly solar metallicity. The left panel shows the position of IRAS 20259 + 4206 as compared with the models for  $Z=0.019$  and masses of 1.8, 2.0 and 2.2  $M_{\odot}$  from Girardi et al. (2000). The blue dashed line is an isochrone of 1.12 Gyrs. The right panel is shows the position of IRAS 02528 + 4350 along with the models for  $Z=0.001$  and masses 0.8, 1.0 and 1.2  $M_{\odot}$ , the shown isochrone is of 3.16 Gyrs.

IRAS 05338 - 3051, IRAS 18025 - 3906 and IRAS 02528 + 4350 have a central absorption flanked by emission peaks on either side displaying each object a weak, strong and moderate P-Cygni structure. Their  $H\alpha$  profiles are very different from star to star. In IRAS 02528 + 4350 the line is almost completely filled and is asymmetric with two emission components in the wings indicative of a complex, non-spherical circumstellar shell, e.g. a circumstellar disc (Klochkova, 2014). Similar profiles are seen in the stars V5112Sgr and BD 48<sup>o</sup>1220=IRAS 05040 + 4820, as shown in figures 2 and 4 of (Klochkova, 2014). The complex  $H\alpha$  profile of IRAS 17279 - 1119 shows a strong P-Cygni structure. The presence of emission features have been interpreted as high mass loss rate (Trams et al., 1989).

Fig. 10 shows the complex structure observed in the Na I  $D_2$  ( $\lambda$ 5890) and  $D_1$  ( $\lambda$ 5895) absorption profiles. We noted that IRAS 17279 - 1119, IRAS 18025 - 3906 and IRAS 18386 - 1253 show multi-component interstellar absorption lines in their spectra. The doublet Na I D lines in IRAS 05338 - 3051, on the other hand, are thinner and show double components in their core.

### 7.3 Evolutionary stages

In order to good estimates of the distances (or luminosities), parallaxes with relative error less than 20% are required. The Gaia DR2 source provides a parallax whose relative error does not exceed 7% only for three objects of our program stars; IRAS 02528 + 4350, IRAS 05338 - 3051 and IRAS 20259 + 4206. For IRAS 17279 - 1119 and IRAS 18025 - 3906 the errors are too large; 27% and 99%, respectively. For IRAS 18386 - 1253 its parallax is not present.

In terms of evolution, we could distinguish three groups among our sample stars. The first one, includes the stars IRAS 02528 + 4350 and IRAS 20259 + 4206. While one of them is moderately iron-deficient and the other show nearly solar abundances, their heliocentric radial velocities are small,  $\alpha$ -elements have solar values and do not display s-process enriched indicating that these are Population I objects. The observed C abundance under NLTE of +0.13 dex seems to indicate that IRAS 02528 + 4350 is evolved and the O enrichment (+0.4 dex) has also been observed for high galactic latitude objects. Likewise, IRAS 20259 + 4206 shows a strong deficiency in carbon which indicates that an additional mechanism to the FDU operates on it. This effect could also indicate that IRAS 20259 + 4206 is probably evolved. However, the Gaia parallaxes indicate luminosities of  $1.06 \pm 0.02$  ( $L_* = 11 \pm 1 L_{\odot}$ ) for IRAS 02528 + 4350 and  $1.46 \pm 0.02$  ( $L_* = 29 \pm 1 L_{\odot}$ ) for IRAS 20259 + 4206, which are values of rather unevolved objects. The effective temperatures are those adopted in Table 2. Evolutionary model tracks in the H-R diagram (HRD) for the compositions [ $Z=0.019$ ,  $Y=0.273$ ] and [ $Z=0.001$ ,  $Y=0.230$ ] are shown in Fig. 11. The evolutionary tracks and isochrones

are from Girardi et al. (2000). In the left panel we observe that an evolutionary track with intermediate-mass of  $2.0 \pm 0.1 M_{\odot}$  and an age of 1.12 Gyr (blue dashed lines) is representative for IRAS 20259 + 4206. In the right panel a track with low-mass of  $1.2 \pm 0.1 M_{\odot}$  and an age of 3.16 Gyr (blue dashed lines) are specific for IRAS 02528 + 4350. The HRD of Fig. 11 suggests that both objects have low-and-intermediate masses that have not reached the RGB. The IRAS two colour diagram, on the other hand, shows that both objects have mid-IR excess at [12]–[25], which could indicate the presence of cold dust due to an extended circumstellar envelope and therefore, they could be confused with evolved objects, i.e. true PAGBs.

In the second evolutionary group we include the stars IRAS 17279 - 1119 and IRAS 05338 - 3051. De Smedt et al. (2016) have confirmed the binary and PAGB nature of IRAS 17279 - 1119. In fact, the luminosity derived from the Gaia parallax leads to a value of  $4.18 \pm 0.26$ . The PAGB model sequences of Miller Bertolami (2016) at  $Z = 0.01$  suggest that this star has initial ZAMS mass of  $\sim 3 M_{\odot}$  and a core mass of  $\sim 0.706 M_{\odot}$ . IRAS 05338 - 3051, on the contrary, shows peculiarities in the observed abundances, e. g. overabundance of s-process elements without an accompaniment of C enrichment. Moreover, IRAS 05338 - 3051 does not show mid-IR excess ([12]–[25] = -0.37), the N (+0.7) is not high enough to explain the C deficiency from the CN cycle and the light and heavy s-process elements have values of +0.47 and +0.53 respectively. Similar peculiarities have also been observed in two previously studied objects; IRAS 06165 + 3158 (S. S. Rao & Girdhar, 2014) and V453 Oph (Deroo et al., 2005). Our abundances are clearly comparable with the observed abundances for V453 Oph. This object is a metal deficient pop. II RV Tauri star with significant enrichment in heavy elements, C deficient and without IR excess. The simulations based on AGB s-process model indicate that C enrichment is inevitable. In this sense, it is not easy to explain these abundances with the current nucleosynthesis models. Deroo et al. (2005) propose several scenarios to explain the peculiar abundances in V453 Oph such as parental cloud, the enrichment by a binary companion and intrinsic s-process enrichment by dredge-up but none of these scenarios explain satisfactorily the observed abundances. More high quality observations may be required to select a possible scenario. Photometrically, Arhipova et al. (2011) have found that the light curve of IRAS 05338 - 3051 exhibits stable sinusoidal variations with amplitude modulations and the pulsation period has remained almost stable for decades. Vickers et al. (2015) have calculated for this object a luminosity of  $L_{*} = 3500 \pm 1500 L_{\odot}$  which is characteristic of the old thin-disk, with age, metallicity and mass in the ranges 3–8 Gyr,  $-0.7$ – $+0.5$  and  $1.1$ – $1.6 M_{\odot}$ . However, we can see that our object is less metallic ( $-1.3$  dex) than the metallicity range proposed for the old thin disk population. This would lead to us to deduce that IRAS 05338 - 3051 rather has a luminosity of the thick disk Population of  $L_{*} = 1700 \pm 750 L_{\odot}$  (or  $3.23 \pm 0.16$ ). The

luminosity of IRAS 05338 - 3051 obtained from the Gaia parallax of  $3.12 \pm 0.06$  is within the uncertainty of luminosity of the thick disk Population. The PAGB model sequences of Miller Bertolami (2016) at  $Z = 0.001$  suggest that IRAS 05338 - 3051 has initial ZAMS mass of  $\sim 0.9 M_{\odot}$  and a core mass of  $\sim 0.533 M_{\odot}$  and an age of  $\sim 5.01$  Gyr. The similarity on observed abundances between V453 Oph and our object seems to indicate that IRAS 05338 - 3051 is a probable PAGB. Extensive radial velocity monitoring is required to verify the binary nature of this object.

The third group contains the stars IRAS 18025 - 3906 and IRAS 18386 - 1253. The two objects show mid-IR excess, their luminosities have not been clearly established and they show peculiarities in their abundance patterns, e.g. IRAS 18025 - 3906 is O-rich and does not show enrichment of s-process elements and IRAS 18386 - 1253 shows a mildly depletion of the refractory elements. The presence of dust around these objects makes difficult the estimation of their distances and/or luminosities are difficult to estimate, and questions the PAGB nature. Therefore, an independent determination of the luminosity is necessary to achieve a better idea of the true nature of these objects. The Gaia source does not provide reliable parallax for neither of the two objects. An alternative to the estimation of the distance and/or luminosity might come from 2MASS photometric calibrations of Molina (2012). These calibrations lead to the distance of  $2805 \pm 363$  pc and a luminosity of  $2.30 \pm 0.11$  ( $L_{*} = 200 \pm 51 L_{\odot}$ ) for IRAS 18025 - 3906 and a distance of  $3267 \pm 422$  pc and a luminosity of  $2.94 \pm 0.11$  ( $L_{*} = 871 \pm 223 L_{\odot}$ ) for IRAS 18386 - 1253 respectively. These luminosities are lower than the expected luminosity of the RGB-tip ( $\lesssim 2500 L_{\odot}$ ) for stars studied in the Magellanic Clouds (SCM and LMC) (Kamath et al., 2014, 2015). This suggests that both objects could have an evolutionary fate totally different from the PAGBs.

In the light of the most recent spectroscopic analyzes in the search of PAGBs candidates in the Magellanic Clouds (SMC and LMC), a new population of evolved, dusty stars identifies as post-RGB objects has been revealed, with luminosities below  $2500 L_{\odot}$ , gravities between 0 to 2, metallicities from  $-2.5$  to  $+0.5$  and masses between  $0.28$  to  $0.45 M_{\odot}$  (Kamath et al., 2014, 2015). The post-RGB are peculiar stars that have interrupted their normal evolution in the RGB phase from a binary mechanism which causes that their intrinsic properties (pulsation, loss-mass, photospheric chemistry, dust-formation, circumstellar envelope morphology, etc) are altered and evolve away from the RGB phase. The final result on these binary evolved objects is the presence of a Keplerian circumbinary disk of gas and dust. See the work of Kamath et al. (2016) for more detailed scenarios of binary formation of the post-RGB objects. Until now, this class of objects has not been clearly identified in the Galaxy, likely due to the lack of accurate measurements of their distances and/or luminosities. However, it cannot be ruled out that some of the galactic PAGB candidates that have not yet been studied turn out to be post-RGB objects.

We suggest that IRAS 18025-3906 and IRAS 18386-1253 are likely members of the post-RGB class. Their abundance patterns seem to indicate that both objects are evolved and within dusty circumstellar environments. Clearly, the luminosities estimated by Molina (2012) are more lower than those suggested by Vickers et al. (2015) when considering the two objects as PAGBs ( $3500 \pm 1500$  and  $6000 \pm 1500 L_{\odot}$ ). This implies that IRAS 18025-3906 and IRAS 18386-1253 may have similar masses and gravities than the known extragalactic post-RGB objects.

## 8 Summary and Conclusions

Our present investigation of a set of six PAGB candidates, five not previously explored, led to confirmation of the PAGB nature of IRAS 05338-3051, as well as two likely Galactic post-RGB candidates such as IRAS 18025-3906 and IRAS 18386-1253, from a detailed atmospheric abundance analysis with high-resolution spectra and their luminosities. IRAS 05338-3051 do not have infrared excess and probably has a binary nature, and IRAS 18025-3906 and IRAS 18386-1253 might be the first Galactic post-RGB objects confused with true PAGBs.

Other objects studied in the sample, IRAS 02528 + 4350 (metal-poor) and IRAS 20259 + 4206 (metal-solar) show signs of being unevolved objects. Although both objects present unconfirmed signs of selective removal, their low radial velocities,  $\alpha$ -elements with abundances nearly solar and lack of s-process elements enrichment, confirm their unevolved nature. Their low mass and luminosity and their gravity larger than 2.0, discard them as probable Galactic post-RGB and confirm that their evolution does not exceed the RGB phase.

## Acknowledgments

We would like to thank Prof. Sunetra Giridhar for useful discussions on abundances and valuable comments on the text, and also for providing the spectra of IRAS 02528 + 4350 and IRAS 17279-1119 used in this study. We are grateful to Dr. Anibal García Hernández and Dr. Olga Zamora for taking the spectrum of IRAS 20259 + 4206 at the Roque de los Muchachos Observatory and to Dr. Bala Sudhakara Reddy for providing us with the McDonald spectrum of IRAS 05338-3051. AAF is indebted to DGAPA-UNAM (México) for a grant through project IN104917. Numerous comments and suggestions made by the anonymous referee are thankfully acknowledged.

## References

- Arellano Ferro, A. (1985, December), *Rev. Mexicana Astron. Astrofis.*, *11*, 113.
- Arellano Ferro, A., Giridhar, S., & Mathias, P. (2001, March), *A&A*, *368*, 250-266.
- Arhipova, V. P., Ikonnikova, N. P., & Komissarova, G. V. (2011, September), *Astronomy Letters*, *37*, 635-648.
- Asplund, M., Grevesse, N., Sauval, A. J., & Scott, P. (2009, September), *ARA&A*, *47*, 481-522.
- Bloecker, T. (1995, July), *A&A*, *299*, 755.
- Bogaert, E. (1994). *Multispectrale studie van de aard en de veranderlijkheid van optisch-heldere sterren met circumstellaire stofschillen*. (Unpublished doctoral dissertation). PhD thesis. Kathol. Univ. Leuven, (1994).
- Bond, H. E. (1991), Chemical Composition of Post-AgB Stars. In G. Michaud & A. V. Tutukov (Eds.), *Evolution of Stars: the Photospheric Abundance Connection* Vol. 145, p. 341.
- Bujarrabal, V., Castro-Carrizo, A., Alcolea, J., & Van Winckel, H. (2015, March), *A&A*, *575*, L7.
- Busso, M., Gallino, R., & Wasserburg, G. J. (1999), *ARA&A*, *37*, 239-309.
- Şahin, T., & Lambert, D. L. (2009, October), *MNRAS*, *398*, 1730-1741.
- Castelli, F., & Kurucz, R. L. (2003), New Grids of ATLAS9 Model Atmospheres. In N. Piskunov, W. W. Weiss, & D. F. Gray (Eds.), *Modelling of Stellar Atmospheres* Vol. 210, p. A20.
- Cohen, M. (1992, June), *AJ*, *103*, 1734-1745.
- de Ruyter, S., van Winckel, H., Maas, T., Lloyd Evans, T., Waters, L. B. F. M., & Dejonghe, H. (2006, March), *A&A*, *448*, 641-653.
- De Smedt, K., Van Winckel, H., Kamath, D., Karakas, A. I., Siess, L., Goriely, S., & Wood, P. (2014, March), *A&A*, *563*, L5.
- De Smedt, K., Van Winckel, H., Kamath, D., Siess, L., Goriely, S., Karakas, A. I., & Manick, R. (2016, March), *A&A*, *587*, A6.
- De Smedt, K., Van Winckel, H., Karakas, A. I., Siess, L., Goriely, S., & Wood, P. R. (2012, May), *A&A*, *541*, A67.
- Deroo, P., Reyniers, M., van Winckel, H., Goriely, S., & Siess, L. (2005, August), *A&A*, *438*, 987-998.
- Deroo, P., van Winckel, H., Min, M. et al. (2006, April), *A&A*, *450*, 181-192.
- Deroo, P., van Winckel, H., Verhoelst, T., Min, M., Reyniers, M., & Waters, L. B. F. M. (2007, June), *A&A*, *467*, 1093-1101.
- Dray, L. M., Tout, C. A., Karakas, A. I., & Lattanzio, J. C. (2003, February), *MNRAS*, *338*, 973-989.
- Eggen, O. J. (1986, April), *AJ*, *91*, 890-918.
- García-Lario, P. (2006), Properties of Post-AGB Stars. In M. J. Barlow & R. H. Méndez (Eds.), *Planetary Nebulae in our Galaxy and Beyond* Vol. 234, p. 63-70.
- García-Lario, P., Manchado, A., Pych, W., & Pottasch, S. R. (1997, December), *A&AS*, *126*, 479-502.



- García-Segura, G., López, J. A., & Franco, J. (2005, January), *ApJ*, 618, 919-925.
- Gezer, I., Van Winckel, H., Bozkurt, Z., De Smedt, K., Kamath, D., Hillen, M., & Manick, R. (2015, October), *MNRAS*, 453, 133-146.
- Gielen, C., van Winckel, H., Min, M. et al. (2011, September), Stable Discs around Galactic and LMC Post-AGB Binaries. In F. Kerschbaum, T. Lebzelter, & R. F. Wing (Eds.), *Why Galaxies Care about AGB Stars II: Shining Examples and Common Inhabitants* Vol. 445, p. 281.
- Gielen, C., van Winckel, H., Reyniers, M. et al. (2009, December), *A&A*, 508, 1391-1402.
- Girardi, L., Bressan, A., Bertelli, G., & Chiosi, C. (2000, February), *A&AS*, 141, 371-383.
- Giridhar, S. (2011), The progress in the study of post-AGB stars. In *Astronomical Society of India Conference Series* Vol. 3, p. 39.
- Giridhar, S., Lambert, D. L., & Gonzalez, G. (2000, March), *ApJ*, 531, 521-536.
- Giridhar, S., Lambert, D. L., Reddy, B. E., Gonzalez, G., & Yong, D. (2005, July), *ApJ*, 627, 432-445.
- Giridhar, S., Molina, R., Ferro, A. A., & Selvakumar, G. (2010, July), *MNRAS*, 406, 290-306.
- Giridhar, S., Rao, N. K., & Lambert, D. L. (1994, December), *ApJ*, 437, 476-484.
- Gonzalez, G., Lambert, D. L., & Giridhar, S. (1997, May), *ApJ*, 481, 452-466.
- Gorlova, N., Van Winckel, H., Ikonnikova, N. P. et al. (2015, August), *MNRAS*, 451, 2462-2478.
- Herwig, F. (2005, September), *ARA&A*, 43, 435-479.
- Hillen, M., Menu, J., Van Winckel, H. et al. (2014, August), *A&A*, 568, A12.
- Hillen, M., Verhoelst, T., Van Winckel, H. et al. (2013, November), *A&A*, 559, A111.
- Hoffmeister, C. (1943, July), *Astronomische Nachrichten*, 274, 36.
- Hu, J. Y., Slijkhuis, S., de Jong, T., & Jiang, B. W. (1993, August), *A&AS*, 100, 413-430.
- Iben, I., Jr., & Renzini, A. (1983), *ARA&A*, 21, 271-342.
- Iben, I., Jr., & Truran, J. W. (1978, March), *ApJ*, 220, 980-995.
- Kamath, D., Wood, P. R., & Van Winckel, H. (2014, April), *MNRAS*, 439, 2211-2270.
- Kamath, D., Wood, P. R., & Van Winckel, H. (2015, December), *MNRAS*, 454, 1468-1502.
- Kamath, D., Wood, P. R., Van Winckel, H., & Nie, J. D. (2016, February), *A&A*, 586, L5.
- Karakas, A. I. (2010, April), *MNRAS*, 403, 1413-1425.
- Karakas, A. I., Marino, A. F., & Nataf, D. M. (2014, March), *ApJ*, 784, 32.
- Klochkova, V. G. (2014, July), *Astrophysical Bulletin*, 69, 279-295.
- Kukarkin, B. V., Kholopov, P. N., Pskovsky, Y. P., Efremov, Y. N., Kukarkina, N. P., Kurochkin, N. E., & Medvedeva, G. I. (1971), The third edition containing information on 20437 variable stars discovered and designated till 1968. In *General Catalogue of Variable Stars, 3rd ed. (1971)*.
- Lind, K., Asplund, M., Barklem, P. S., & Belyaev, A. K. (2011, April), *A&A*, 528, A103.
- Lind, K., Bergemann, M., & Asplund, M. (2012, November), *MNRAS*, 427, 50-60.
- Lodders, K. (2003, July), *ApJ*, 591, 1220-1247.
- Maas, T., Van Winckel, H., & Waelkens, C. (2002, May), *A&A*, 386, 504-516.
- Marigo, P., Bressan, A., Nanni, A., Girardi, L., & Pumo, M. L. (2013, September), *MNRAS*, 434, 488-526.
- Miller Bertolami, M. M. (2016, April), *A&A*, 588, A25.
- Molina, R. E. (2012, April), *Rev. Mexicana Astron. Astrofis.*, 48, 95-107.
- Molina, R. E. (2018, October), *Rev. Mexicana Astron. Astrofis.*, 54, 397-408.
- Molina, R. E., Giridhar, S., Pereira, C. B., Arellano Ferro, A., & Muneer, S. (2014, October), *Rev. Mexicana Astron. Astrofis.*, 50, 293-306.
- Nakanishi, K., Takata, T., Yamada, T. et al. (1997), *ApJS*, 112, 245-270.
- Pereira, C. B., & Miranda, L. F. (2007, January), *A&A*, 462, 231-236.
- Preite-Martinez, A. (1988, December), *A&AS*, 76, 317-330.
- Ramírez, I., & Allende Prieto, C. (2011, December), *ApJ*, 743, 135.
- Rao, N. K., & Reddy, B. E. (2005, February), *MNRAS*, 357, 235-241.
- Rao, S. S., & Giridhar, S. (2014, April), *Rev. Mexicana Astron. Astrofis.*, 50, 49-65.
- Rao, S. S., Giridhar, S., & Lambert, D. L. (2012, January), *MNRAS*, 419, 1254-1270.
- Reddy, B. E., Lambert, D. L., Gonzalez, G., & Yong, D. (2002, January), *ApJ*, 564, 482-494.
- Reyniers, M., van de Steene, G. C., van Hoof, P. A. M., & van Winckel, H. (2007, August), *A&A*, 471, 247-254.
- Reyniers, M., Van Winckel, H., Biémont, E., & Quinet, P. (2002, November), *A&A*, 395, L35-L38.
- Reyniers, M., Van Winckel, H., Gallino, R., & Straniero, O. (2004, April), *A&A*, 417, 269-281.
- Sackmann, I.-J., & Boothroyd, A. I. (1992, June), *ApJ*, 392, L71-L74.
- Samus, N. N., Kazarovets, E. V., Durlevich, O. V., Kireeva, N. N., & Pastukhova, E. N. (2009, January), *VizieR Online Data Catalog*, 1.
- Schmidt-Kaler, T. (1982), , 2.
- Silva, A. M., Azcarate, I. N., Poppel, W. G. L., & Likkell, L. (1993, August), *A&A*, 275, 510.
- Snedden, C. A. (1973). *Carbon and Nitrogen Abundances in Metal-Poor Stars*. (Unpublished doctoral dissertation). THE UNIVERSITY OF TEXAS AT AUSTIN.
- Straizys, V. (1982), *Metal-deficient stars*.
- Suárez, O., García-Lario, P., Manchado, A., Manteiga, M., Ulla, A., & Pottasch, S. R. (2006, October), *A&A*, 458, 173-180.
- Suárez, O., Gómez, J. F., & Morata, O. (2007, June), *A&A*, 467, 1085-1091.

- Szczerba, R., Siódmiak, N., Stasińska, G., & Borkowski, J. (2007, July), *A&A*, 469, 799-806.
- Szczerba, R., Yung, B. H. K., Sewiło, M., Siódmiak, N., & Karska, A. (2017, October), AGB and post-AGB objects in the outer Galaxy. In X. Liu, L. Stanghellini, & A. Karakas (Eds.), *Planetary Nebulae: Multi-Wavelength Probes of Stellar and Galactic Evolution* Vol. 323, p. 369-370.
- Takeda, Y., & Takada-Hidai, M. (1998, December), *PASJ*, 50, 629-638.
- Trams, N. R., Waters, L. B. F. M., Lamers, H. J. G. L. M., Waelkens, C., Geballe, T. R., & The, P. S. (1991, February), *A&AS*, 87, 361-382.
- Trams, N. R., Waters, L. B. F. M., Waelkens, C., Lamers, H. J. G. L. M., & van der Veen, W. E. C. J. (1989, July), *A&A*, 218, L1-L4.
- Tull, R. G., MacQueen, P. J., Sneden, C., & Lambert, D. L. (1995, March), *PASP*, 107, 251-264.
- van Aarle, E., Van Winckel, H., De Smedt, K., Kamath, D., & Wood, P. R. (2013, June), *A&A*, 554, A106.
- van Aarle, E., van Winckel, H., Lloyd Evans, T., Ueta, T., Wood, P. R., & Ginsburg, A. G. (2011, June), *A&A*, 530, A90.
- van der Veen, W. E. C. J., & Habing, H. J. (1988, April), *A&A*, 194, 125-134.
- van der Veen, W. E. C. J., Trams, N. R., & Waters, L. B. F. M. (1993, March), *A&A*, 269, 231-241.
- Van Winckel, H. (1997, March), *A&A*, 319, 561-577.
- van Winckel, H. (2003), *ARA&A*, 41, 391-427.
- Van Winckel, H., Decin, L., & Waelkens, C. (1997), The chemical composition of post-AGB stars. In T. R. Bedding, A. J. Booth, & J. Davis (Eds.), *IAU Symposium* Vol. 189, p. 176.
- Van Winckel, H., Jorissen, A., Gorlova, N. et al. (2010), *Mem. Soc. Astron. Italiana*, 81, 1022.
- van Winckel, H., Lloyd Evans, T., Briquet, M. et al. (2009, October), *A&A*, 505, 1221-1232.
- Van Winckel, H., Waelkens, C., & Waters, L. B. F. M. (1995, January), *A&A*, 293.
- Vassiliadis, E., & Wood, P. R. (1993, August), *ApJ*, 413, 641-657.
- Venn, K. A. (1995, August), *ApJ*, 449, 839.
- Venn, K. A., & Lambert, D. L. (1990, November), *ApJ*, 363, 234-244.
- Venn, K. A., Puzia, T. H., Divell, M., Côté, S., Lambert, D. L., & Starkenburg, E. (2014, August), *ApJ*, 791, 98.
- Vickers, S. B., Frew, D. J., Parker, Q. A., & Bojičić, I. S. (2015, February), *MNRAS*, 447, 1673-1691.
- Waters, L. B. F. M., Trams, N. R., & Waelkens, C. (1992, September), *A&A*, 262, L37-L40.
- Yoon, D.-H., Cho, S.-H., Kim, J., Yun, Y. j., & Park, Y.-S. (2014, March), *ApJS*, 211, 15.